JACS
JOURNAL OF THE AMERICAN CHEMICAL SOCIETY
Article
Cite This: J. Am. Chem. Soc. 2019, 141, 6030−6047
pubs.acs.org/JACS

Cross Conjugation in Polyenes and Related Hydrocarbons: What Can Be Learned from Valence Bond Theory about Single-Molecule Conductance?

Junjing Gu,[†] Wei Wu,*[,†] Thijs Stuyver,*[,‡,§] David Danovich,[‡] Roald Hoffmann,*[,∥] Yuta Tsuji,[⊥] and Sason Shaik*[,‡]

[†]State Key Laboratory of Physical Chemistry of Solid Surfaces, iChEM, Fujian Provincial Key Laboratory of Theoretical and Computational Chemistry and College of Chemistry and Chemical Engineering, Xiamen University, Xiamen, Fujian 361005, China

[‡]Department of Organic Chemistry and the Lise Meitner-Minerva Centre for Computational Quantum Chemistry, The Hebrew University, Jerusalem 91904, Israel

[§]Algemene Chemie, Vrije Universiteit Brussel, Pleinlaan 2, 1050 Brussels, Belgium

[∥]Department of Chemistry and Chemical Biology, Baker Laboratory, Cornell University, Ithaca, New York 14853, United States

[⊥]Institute for Materials Chemistry and Engineering and IRCCS, Kyushu University, Nishi-ku, Fukuoka 819-0395, Japan

Supporting Information

ABSTRACT: This study examined the nature of the electronic structure of representative cross-conjugated polyenes from a valence bond (VB) perspective. Our VBSCF calculations on a prototypical dendralene model reveal a remarkable inhibition of the delocalization compared to linear polyenes. Especially along the C−C backbone, the delocalization is virtually quenched so that these compounds can essentially be considered as sets of isolated butadiene units. In direct contrast to the dendralene chains, quinodimethane compounds exhibit an enhancement in their delocalization compared to linear polyenes. We demonstrate that this quenching/enhancement of the delocalization is inherently connected to the relative weights of specific types of long-bond VB structures. From our ab initio treatment, many localization/delocalization-related concepts and phenomena, central to both organic chemistry and single-molecule electronics, emerge. Not only do we find direct insight into the relation between topology and the occurrence of quantum interference (QI), but we also find a phenomenological justification of the recently proposed diradical character-based rule for the estimation of the magnitude of molecular conductance. Generally, our results can be conceptualized using the "arrow-pushing" concept, originating from resonance theory.

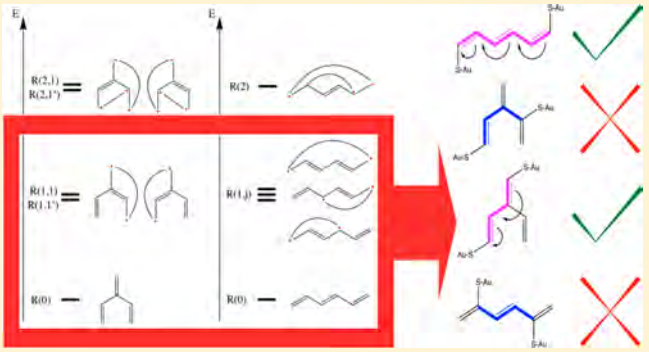

1. INTRODUCTION

Cross-conjugation in polyenes and other unsaturated hydrocarbons is a ubiquitous phenomenon in organic chemistry.[1,2] Broadly speaking, the term "cross-conjugation" has been applied to any compound containing branched conjugated systems.[3] Figure 1 exemplifies some of these molecules, like [*n*]-dendralenes, [*n*]radialenes, fulvene, and *p*-quinodimethane, which possess different cross-conjugated topologies.[1]

Cross-conjugation has been linked to a disjointed electronic communication or delocalization and thus forms a natural counter to linear conjugation, wherein the delocalization is thought to be significant.[4−7] Over the past decade, the interest in this phenomenon of impeded electronic communication has soared due to the demonstrated connection between the cross-conjugated structural motif and the occurrence of (destructive) quantum interference (QI) in molecular electronics.[8−11] Furthermore, compounds exhibiting extensive cross-conjugation (dendralenes, radialenes, fulvenes, etc.; cf. Figure 1) have become experimentally available due to impressive advances in synthesis[12−16] and are not anymore "a neglected family of hydrocarbons".[15] There have been several theoretical and computational studies on the nature of cross-conjugation vis-à-vis linear conjugation.[2,4,15,17−25] The theoretical treatments so far used by and large a combination of Hückel MO theory and graph theory,[2,4,21,23] or resonance theory and graph theory.[24] However, an in-depth understanding of the origin of some of the remarkable properties associated with this phenomenon is still necessary in terms of computational quantum chemistry. As such, we provide herein insights coming from valence bond (VB) theory on the nature of cross-conjugation vis-à-vis linear

Received: February 6, 2019
Published: March 19, 2019

DOI: 10.1021/jacs.9b01420
J. Am. Chem. Soc. 2019, 141, 6030−6047

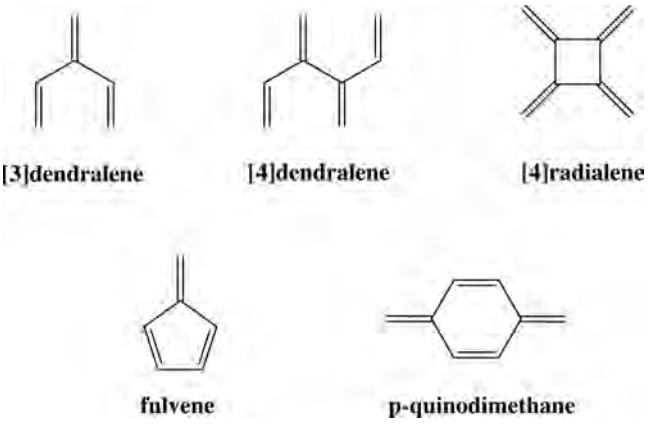

Figure 1. Examples of compounds involving extensive cross-conjugation.

conjugation as in linear polyenes. Let us provide first an overview of the topic.

The origin of the limited interest initially directed toward the purposeful design of cross-conjugated compounds can be attributed to the absence of obvious applications for such compounds. Thus, whereas linear polyenes play a vital role in life-sustaining systems (cf. the mechanism of vision and light harvesting systems) and as conducting polymers,[7,26] extensively cross-conjugated compounds seemed at first to be of fairly limited applicability. Nevertheless, these polyenes have been recognized as suitable starting points for syntheses involving multiple Diels–Alder additions already early on.[1,11,27] Even though some short dendralene derivatives (arguably the archetypical class of cross-conjugated compounds) were already synthesized as early as at the start of the twentieth century,[12,28,29] a general route to dendralenes of varying length was only achieved about a century later.[13,14,30,31] Several synthetic routes toward the design of cyclic analogues of dendralenes (radialenes and fulvenes and their derivatives) were developed during the 1970s and later; yet even for these classes of compounds, the structural diversity was, until recently, fairly small.[32−40] Another class of molecules involving some cross-conjugation are the quinoid compounds. Given the biological importance of quinone and other quinoid structures,[41−43] the chemistry of these compounds has been studied more extensively.[44−48]

Next to their mentioned usefulness as building blocks for complex compounds involving Diels–Alder reactivity, cross-conjugated compounds (dendralenes) have also received some attention due to their fairly large and constant HOMO–LUMO gaps which do not decrease with the increasing dendralene size. This suggests also small changes in excitation energies, ionization potentials, and electron affinities with respect to the system size.[3] In fact, Fowler et al. theoretically determined dendralene to be the polyene oligo-/polymer with the maximal HOMO–LUMO gap on the basis of a variable neighborhood search.[49] Furthermore, Saglam et al. came to the intriguing conclusion that for a range of dendralenes of varying length, a common UV–vis absorption maximum could be measured which corresponds to the absorption maximum of 1,3-butadiene.[16] Tykwinski and co-workers considered the suitability of perphenylated isopolydiacetylene (*iso*-PDA), a dendralene analogue, as an optoelectronic material due to its enhanced second hyperpolarizability (γ). The observed superlinear increase in γ (i.e., the relationship corresponds to a power law) was attributed to the helical conformation of perphenylated *iso*-PDA caused by the extensive steric strain present in this compound (such steric hindrance is a general feature of cross-conjugated compounds; vide infra).[50] Nevertheless, as mentioned before, the use of cross-conjugated compounds as building blocks for materials has been rather limited. However, this limitation vanished in the wake of the recent boom in the field of single-molecule electronics.

Single-molecule electronics involves the study and the design of electronic devices such as wires, switches, diodes, transistors, etc. at the molecular scale.[51] In a typical single-molecule electronics experiment, molecules are assembled between two conducting (gold) surfaces so that a molecular junction is formed. The measured I/V profile for the resulting junction is intimately connected to the electronic structure of the molecule involved.[52]

One of the phenomena originating from single-molecule electronics (appealing strongly to the imagination of many chemists) is (destructive) quantum interference.[53,54] Destructive QI features are a reflection of the wave nature of electrons and can be defined as antiresonances in the transmission spectrum associated with the molecular junction, which are caused by the mutual cancellation of the different transport channels through the molecule in the coherent transport regime. QI features located in the vicinity of the Fermi level of the studied molecular junction lead to the measurement of a reduced conductance under small bias.[54] Over the past decade, a clear connection between cross-conjugation and destructive quantum interference has been established.[8−10] The phenomenon of QI has been invoked, among other effects, to explain the observed reduction of the conductance of a benzene molecule contacted in the *meta* configuration as compared to the more distant *para* configuration and of (cross-conjugated) anthraquinone as compared to its linearly conjugated analogue anthracene.[9,55,56] Furthermore, recent calculations performed by one of the authors of the present study (TS) demonstrated that cross-conjugation features in a molecular structure generally play the role of barriers to coherent electronic current. Whenever these barriers seal off all conjugated paths within the molecule from contact to contact, QI will arise in the region around the Fermi level, and if this is not the case, the barriers seal off parts of the molecule so that these molecular fragments can effectively be neglected in the theoretical calculation of the transmission spectrum.[18]

Ever since the initial observation of QI and the establishment of its connection to cross-conjugation, a variety of models and rules have been developed to explain and predict the occurrence of this phenomenon. However, many of these rules employ a language that is at times far removed from the natural language used by chemists or involve chemical concepts based on very approximate and/or qualitative descriptions of the molecular electronic structure.[53,57−67]

In this work, we take a fresh look at the electronic structure of cross-conjugated compounds starting from a VB perspective. It will be shown that the delocalization of both cross- and linear-conjugated polyenes is caused primarily by the mixing of the available long-bond structures into the fundamental Lewis structure of the respective polyene, in affinity with the study of Ray Dias.[24] As such, it will be demonstrated that an intuitive explanation for many of the remarkable properties and observations outlined above comes out in a natural way from this chemically oriented treatment. VB theory is especially appealing to this end, since it offers unrivaled conceptual insight into the delocalization characteristics of compounds.[7]

DOI: 10.1021/jacs.9b01420
J. Am. Chem. Soc. 2019, 141, 6030−6047

Target Molecules. Recently, some of the authors of the present study demonstrated that VB theory reveals the hidden delocalized nature of (linearly conjugated) polyenes $C_{2n}H_{2n+2}$, **1** in Chart 1.[7] The theoretical treatment showed that starting with

Chart 1. 1, Linear Polyenes; 2, [*m*]Dendralene; 3, [*m*]*o*-Quinodimethane; 4, [*m*]*p*-Quinodimethane

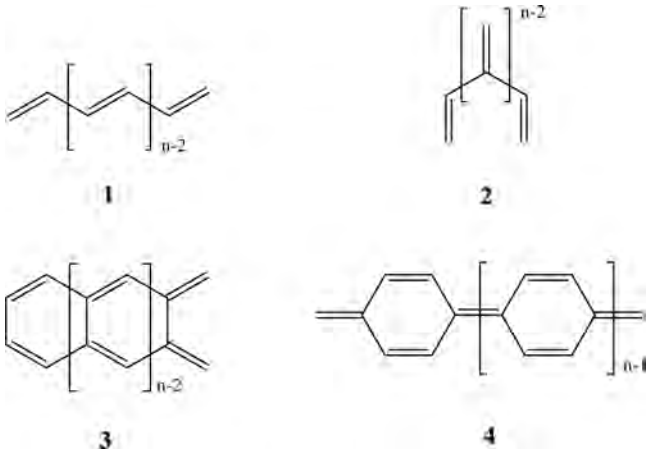

n = 5−6, *the polyene's wave function is mainly a shifting 1,m-diradicaloid* (*m* ≥ 4), a character that increases as the chain length increases, while the contribution of the fundamental Lewis structure with alternating double and single bonds decays quite fast and becomes minor relative to the diradicaloid pack. The same study showed how, nevertheless, *it is this wave function that predicts that polyenes will still exhibit alternating short/long CC bonds, like the fundamental structure, which contains alternating double/single bonds*. As such, the present VB contribution should be considered as a second chapter in our ongoing study of delocalization phenomena in conjugated systems.

Below, we will focus specifically on model cross-conjugated systems, which are depicted in Chart 1. The main targets are the planar dendralenes, **2**, which will be compared to the linear polyenes, **1**, as well as to a few members of the *o*- and *p*-quinodimethane species, **3** and **4**. It is seen that both the linear polyenes **1** and the dendralenes **2** may be viewed as polymers having *s-trans* butadienic building blocks, which exhibit different connectivities; **1** has a contiguous delocalization path, while for **2** the C=C bonds in the Lewis structure form butadiene segments that are connected via their middle C−C bond but are otherwise disjointed. The quinodimethanes (QDMs) have more complex themes of cross-conjugated double chains. The *o*-QDMs **3** can be viewed as two *s-transoid* linear polyene chains cross-conjugated at their vinylic carbon atoms, while the *p*-QDMs involve an alternating *s-transoid*−*cisoid* polyene capped in a cross-conjugated manner with double bonds. Alternatively, *o*-QDMs **3** may be viewed as containing fused *s-cis* butadienic units.

The cross-conjugated target molecules **2**−**4**, will be treated by the same VB methodology as used before[7] for the linear polyenes, **1**, i.e., the valence bond-self-consistent field (VBSCF) method,[70] using a VB-structure set of canonical structures, called the Rumer structures.

2. METHODS

Geometry optimization of the various species was carried out using B3LYP/D95V as implemented in Gaussian 09 program.[68,69] We tried also MP2 and other basis sets. As in the previous study (ref 7), B3LYP gave here results compatible with MP2. All these results are relegated to the Supporting Information (section I).

All the VB calculations were carried out at the VBSCF method[70] with the XMVB code, which is an ab initio valence bond program.[71] The D95V basis set was used for most of the cases. As before, we used also STO-6G for comparison and for the largest systems.[72] The delocalization energy for butadiene was tested before[7] with other basis sets including cc-pVTZ, which gave results virtually identical to D95V.[73]

2.1. The VBSCF Method. The VBSCF method uses a wave function that is a linear combination of VB structures Φ_K with coefficient C_K as shown in eq 1,

$$\Psi = \sum_K C_K \Phi_K \tag{1}$$

where each VB structure is a multideterminantal wave function corresponding to a specific chemical structure, and each VB determinant is constructed from occupied atomic orbitals (here, the $2p_\pi$ orbitals, the generators of the π system). The coefficients C_K are determined by solving the secular equation in eq 2, in the usual variational procedure:

$$\mathbf{HC} = E\mathbf{MC} \tag{2}$$

Here **H**, **M**, **C** are respectively the Hamiltonian, overlap, and coefficient matrices, while E is the total energy of the system (including the σ frame). The variational procedure involves a double optimization of the coefficients C_K, as well as the orbitals of the VB structures, in a given atomic basis set. The σ-frame is treated as a set of doubly occupied MOs (taken from the corresponding Hartree−Fock wave function) that are optimized during the VBSCF procedure. Thus, the VBSCF method is analogous to CASSCF in the sense that both methods optimize structure coefficients (cf. the C_K's in eq 1) as well as the orbitals within the used atomic basis set. We use here the double zeta D95V and the STO-6G basis sets.[69,72]

The VB structures Φ_K are the Rumer structures assembled from VB determinants.[7,74] Rumer structures are the canonical structures, which for a polyene $C_{2n}H_{2n+2}$ constitute all the linearly independent modes of pairing the $2n$ π-electrons into n-pairs. For a general polyene/dendralene $C_{2n}H_{2n+2}$ in a singlet spin state, there exist m Rumer structures in the structure-set given in eq 3:

$$m = \binom{2n}{n} - \binom{2n}{n-1} \tag{3}$$

Diagonalization of the Rumer basis set provides a spectrum of covalent states, the lowest of which is the ground state, which is the focus of the present paper. A critical set of Rumer structures is the block in which a short π-bond is being broken and replaced by a long-bond, which can be of variable lengths (e.g., 1,4; 1,6; etc.).[7] The number of Rumer structures in this block depends on the conjugation-paths types available to the π-electrons.

2.2. Types of Atomic Orbitals in VBSCF. In describing the VB structures, one can use atomic orbitals (AOs), such that the Rumer structures will be purely covalent. This level of calculations is referred to as VBSCF(AO-C), where C means that we used only covalent Rumer structures. Our tests for dendralenes showed that using these orbitals does not lead to correct trends in the series (see section II in the Supporting Information). What the VBSCF(AO-C) method misses are ionic structures. However, as argued before in ref 7, adding explicitly the ionic structures, for example, in [4]dendralene, C_8H_{10}, generates a complete set of 1764 VB structures. Thus, considering all the ionic structures becomes quickly impractical for our study that goes all the way to $C_{16}H_{18}$.

To avoid this multitude of ionic structures, there are ways to account for these structures effectively while conserving the original number of Rumer structures. This is achieved by allowing the AOs to have small delocalization tails on atoms other than the one the AO "belongs" to. In this manner, the formally covalent Rumer structures, which, so-to-speak, are impregnated with ionic structures (see pp 40−42 in ref 74.).

DOI: 10.1021/jacs.9b01420
J. Am. Chem. Soc. 2019, 141, 6030−6047

One such set of orbitals is called BDO,[75,76] where BDO stands for a bond-distorted-orbital in which each AO on a given carbon atom is allowed to have a tail *only on* the atom to which it is bonded. Some of these BDOs are shown in Figure 2 for the smallest dendralene, C_6H_8.

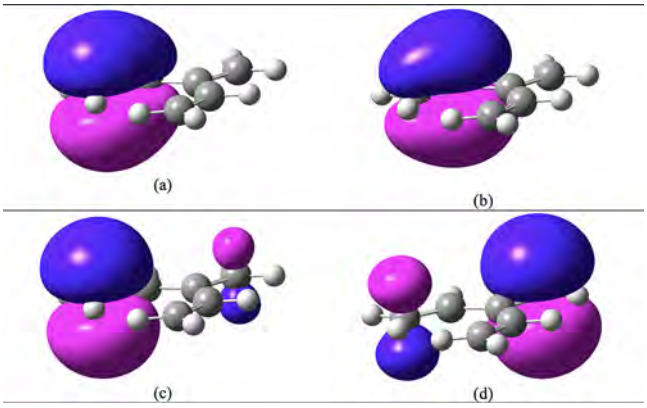

Figure 2. BDOs for C_6H_8: (a) centered on C1 and bonded with C2, (b) centered on C2 and bonded with C1, (c) centered on C1 with a tail on C4, (d) centered on C4 with a tail on C1. The relatively removed tails bring about 1,4-ionic structures and were addressed before in ref 7 (consult also Appendix 2 in the Supporting Information).

We shall refer to this method as VBSCF(BDO-C) where the C denotes that the number of Rumer structures is identical to the covalent Rumer set (note that even though the STO-6G basis functions are single-ζ orbitals, still during the BDO optimization, the tails will become different for different Rumer structures). As such, the VBSCF(BDO-C) level involves implicitly all the short-ranged ionic structures (cf. Appendix 1 in the Supporting Information) and is generally reliable for polyenes and conjugated systems. This is the standard method used in this study. Another set of orbitals, called overlap-enhanced orbitals (OEOs), which do not limit the tails to the bonded atoms, lead to VBSCF(OEO-C), which includes explicitly all the ionic structures.[7] This method was used here, albeit scantly.

Since all the molecules in this study have singlet ground states, the paired electrons over two π-BDOs are singlet-pairs. When in a given Rumer structure, the pairing involves nonconnected carbon atoms, such as 1−4 in linear polyenes, or even more distant pairing, all the way to 1−2n pairs for $C_{2n}H_{2n+2}$, we refer to these as long-bonds, and the corresponding structures are called "diradicaloid structures".

2.3. The Rumer Structure-Set for Dendralenes. The construction of linearly independent Rumer structures requires an atomic connectivity-cycle, without any crossing bonds (or connections). These Rumer structures can be very easily constructed for linear polyenes, as shown in ref 7. However, for cross-conjugated molecules the generation of the corresponding linearly independent Rumer structures is somewhat less intuitive. To bypass the difficulties, we generate for a given dendralene molecule an auxiliary structure that has well-known Rumer structures. We then map these auxiliary Rumer structures unto the dendralene structure and obtain the corresponding Rumer structures for the dendralene.

How this is done is demonstrated in Figure 3 for the smallest [3]dendralene, C_6H_8. In the first step, in Figure 3a, we transpose the position of the pivot-atom, numbered as 1 and marked in red, and we create an auxiliary hexagon, in which we keep the atom-numbering system as in the actual dendralene. Since a hexagonal array of six 2p AOs (BDOs) leads to five Rumer structures (two Kekulé types and three Dewar types), seen on the left-hand side in Figure 3b, we first draw these Rumer structures and then we transform the structures back unto the dendralene structure, keeping the connectivity of the atoms as in the dendralene. The process generates one fundamental Rumer, $R(0)$, a block of two symmetry-related Rumers with one long-bond, labeled as $R(1,j)$, j = 1, 1′, where j is an index of the Rumer structure in the block,

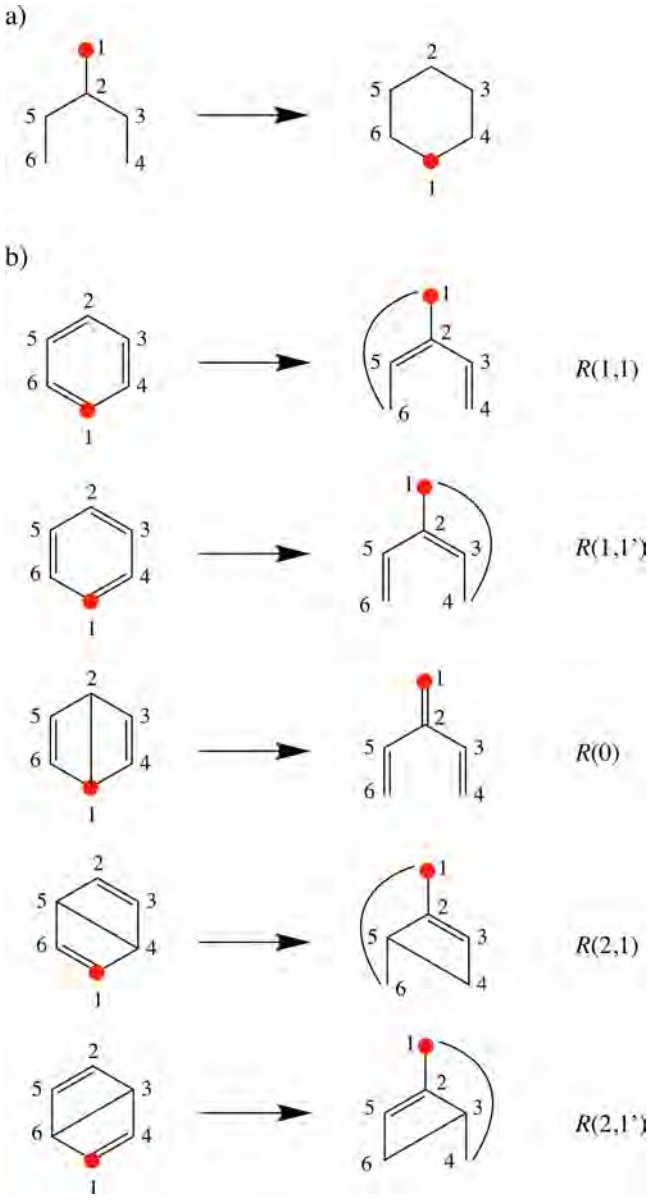

Figure 3. π−Rumer structures for the C_6H_8 dendralene: (a) creating the auxiliary structure, a hexagon, by transposing the C1 (in red) downward by 180°; (b) generating on the left the Rumer structures for the auxiliary hexagon (on the left) and mapping these structures back to the dendralene connectivity (on the right).

and a second block of two symmetry-related Rumer structures having two long-bonds, hence, $R(2,j)$, j = 1, 1′.

Figure 4a shows the energy spectrum of these Rumer structures for [3]dendralene, assuming uniform C−C bond lengths, for the sake of convenience. Thus, we have three blocks of Rumer structures, which are ordered by the number of long-bonds; the lowest is the fundamental structure, $R(0)$, which has zero long-bonds. Above it, a set of two Rumer structures with one long-bonds, $R(1,j)$, where the second index j involves symmetry-related structures, numbered as 1 and 1′. Finally, there is a block of two symmetry-related Rumer structures, which have two long-bonds, and are labeled as $R(2,1)$ and $R(2,1')$. It is seen, in Figure 4b, that the linear polyene, having the same carbon count, has three Rumer structures with one long-bond (1,4- or 1,6 long-bonds) while only one with two long-bonds. As we explained in detail in our previous paper (ref 7), generating one long-bond creates a gap between the two respective Rumer structures with a magnitude given by of (3/2)λ, where λ is the π-bond energy (approximately 60−70 kcal/mol). With such an energy gap, it is clear that the dendralene will exhibit less

DOI: 10.1021/jacs.9b01420
J. Am. Chem. Soc. 2019, 141, 6030−6047

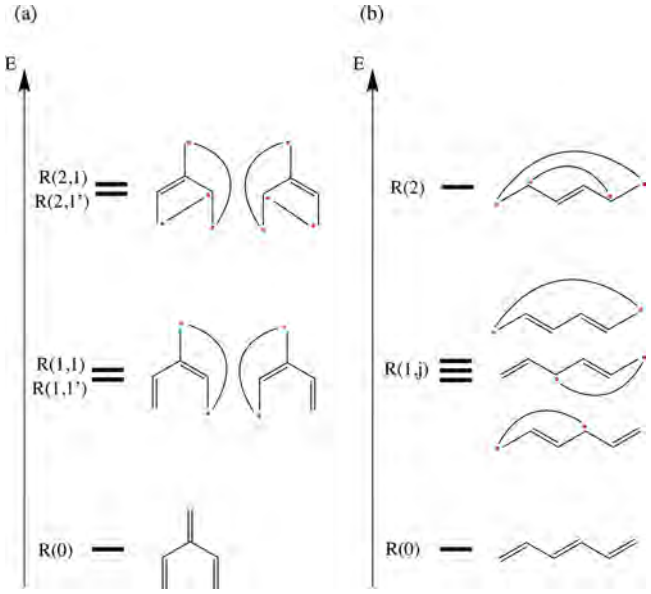

Figure 4. Energy spectrum of Rumer structures for molecules with uniform C−C bond lengths: (a) C_6H_8 dendralene and (b) C_6H_8 linear polyene.

significant mixing of the excited Rumer structures into the fundamental one, $R(0)$.

Generalization of the auxiliary-structure method for generating Rumer structures for dendralene, as well as the full sets of Rumer structures from a few members of the *o*- and *p*-QDMs, is outlined in the Supporting Information (sections III and Appendix 3). The XMVB program[71] generates the Rumer structures automatically.

3. RESULTS

Below, we present our computational results. We start by addressing the validity of our structural model for the dendralenes and subsequently assess the extent of delocalization in these compounds through a variety of indicators. Among others, we consider the signatures of localization found in the geometries and consider total π-energies (E_π), delocalization energies (ΔE_{del}), and the respective relative weights of the fundamental Rumer and diradical structures in the wave function as well as HOMO−LUMO and singlet−triplet gaps. Finally, we turn to the *o*-quinodimethanes and *p*-quinodimethanes (*o*- and *p*-QDMs) and perform an analogous analysis for these compounds before turning to a critical evaluation of the origin of the observed trends in (de)localization and how our findings can be connected to the transport properties of these molecules.

3.1. Designing a Structural Model for Dendralenes.

The geometry optimization (using B3LYP/D95V) shows that [*n*]dendralenes, $n = 3-6$, are all nonplanar (see Table S1 in the Supporting Information). For the smallest member, [3]-dendralene, the experimental electron diffraction (ED) data reveals a skewed *trans*−*cisoid* form with dihedral angle of 39.3°.[17] B3LYP and MP2 calculations with the D95V and aug-cc-pVTZ basis sets reasonably reproduce the experimental skewed structure. Figure 5a shows the ED- and computed-structural data along with relative energies of the skewed and planar structures. It is seen that compared with linear polyenes, the short C=C bonds are very slightly shorter, 1.34−1.37 Å, while the C−C bonds are longer, 1.48−1.5 Å. The geometric details for the planar [3]dendralene conformer, which are shown in Figure 5b, disclose very small changes.

In order to understand the origins of the skewing distortion from planarity, as opposed to the linear polyenes, we used VBSCF(BDO-C)/D95V calculations of the fundamental

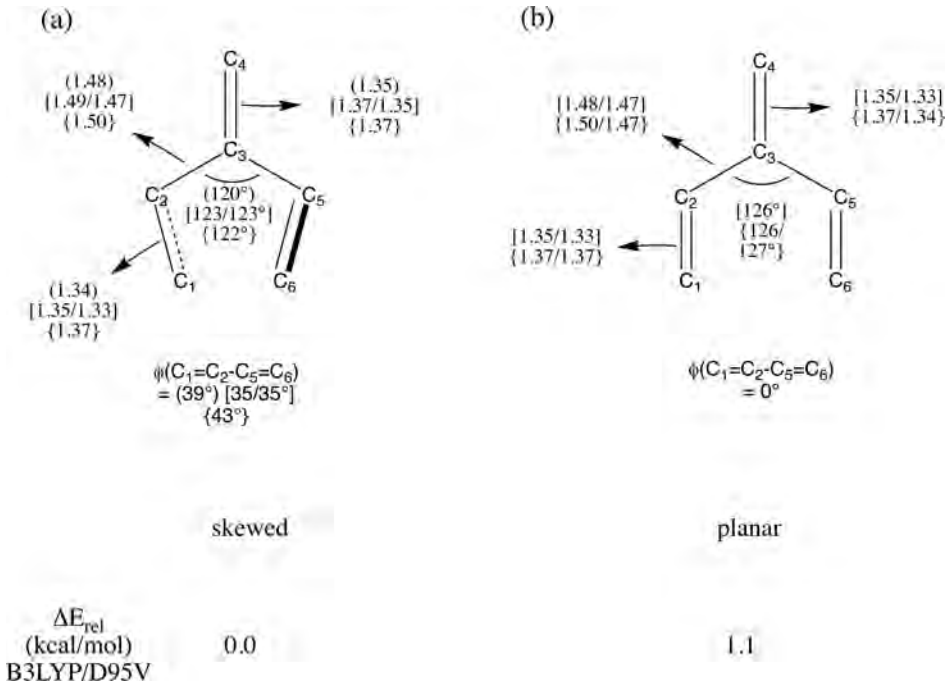

Figure 5. Geometric features of [3]dendralene. (a) Skewed form. Data for each geometric parameter are given in the following order: (experiment), [B3LYP D95V/cc-aug-pVTZ], {MP2 D95V/aug-cc-pVTZ}. (b) Planar form with data given as [B3LYP D95V/cc-aug-pVTZ], {MP2 D95V/aug-cc-pVTZ}. All bond lengths are in Å and angles in degrees. ΔE_{rel} is the relative energy (in kcal/mol) of the two conformers at the B3LYP/D95V level.

DOI: 10.1021/jacs.9b01420
J. Am. Chem. Soc. 2019, 141, 6030−6047

Rumer structure, $R(0)$ of the [3]dendralene, and found that $R(0)$ by itself prefers skewing (by 3.3 kcal/mol; Table S5). Using the recently developed energy decomposition analysis (EDA)[77,78] shows that ∼1.6 kcal/mol out of the total energy difference is due to H···H repulsion of the two CH_2 terminals (C1 and C6). The rest comes from the $\pi-\pi$ Pauli repulsion of the π-bonds. A similar conclusion was reached in ref 7 for the central bond in butadiene. Furthermore, in accord with a recent study by McCarthy et al.,[79] we verified here using VBSCF(BDO-C)/D95V that in *s-cis* butadiene, the skewed structure (close to the gauche conformer) is slightly preferred over the planar one (see Appendix 1 in the Supporting Information), and the preference is dominated by the fundamental structure, $R(0)$.

As a final test, we calculated for the planar and skewed conformers of [3]dendralene, the delocalization energy (ΔE_{del}), and the weight of the fundamental Rumer structure, $W(R(0))$, in the corresponding VBSCF(BDO-C)/D95V wave functions (Tables S2 and S3). The results are depicted in Figure 6. It is

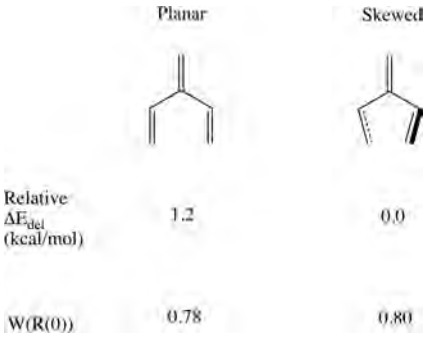

Figure 6. Relative delocalization energies in kcal/mol ($\Delta E_{del} = E_{vb,full} - E_{R(0)}$) at VBSCF(BDO-C)/D95V level, and weights of the fundamental Rumer structure [$W(R(0)$], in the corresponding wave functions.

seen that the planar conformer is very slightly more delocalized than the skewed form, by 1.2 kcal/mol, and in a fully consistent manner this conformer has a smaller weight in $R(0)$.

Clearly, therefore, all the above computational tests show that the planar structure of [3]dendralenes is slightly, if at all, more delocalized than the optimal nonplanar form. As such, the planar conformers of [n]dendralene may serve as reasonable upper-bound delocalized models for the skewed structures (cf. ref 7; see for example the discussion of the skewed rotational TS for *s-trans* butadiene) for the purpose of comparing cross-conjugation with linear-conjugation.

3.2. Indicators of Localization in Dendralenes. A gauge of the relative delocalization of the two polyene families that emerges from molecular orbital (MO) theory is the HOMO−LUMO energy gaps, $\Delta E_{HOMO-LUMO}$. Similarly, the singlet−triplet excitation energy, ΔE_{ST}, of a given polyene indicates the potential for developing diradical character in the singlet ground state. Although both criteria are indirect, we nevertheless tested them here because we aim to increase the insight from both possible approaches (VB and MO). Our results (see Tables S18 and S19) show that while the $\Delta E_{HOMO-LUMO}$(B3LYP/D95V) for linear polyenes drops from 100.5 to 57.0 kcal/mol, in going from C_6H_8 to $C_{16}H_{18}$, the same value for cross-conjugated polyenes remains almost invariant along the series, 112.7−117.7 kcal/mol. Similarly, ΔE_{ST}(B3LYP/D95V) varies for C_6H_8 to $C_{16}H_{18}$ linear polyenes in the range of 43.3−19.1 kcal/mol, whereas for cross-conjugated polyenes, this value remains virtually constant, 52.4−58.9 kcal/mol. While these criteria already demonstrate that electronic communication is impeded in the cross-conjugated polyene family, we shall proceed to look at geometric features and then use VB theory which provides directly the delocalization energies in a quantitative manner and enables at the same time a significant insight into these numbers.

Geometric Features of Planar [n]Dendralenes (n = 3−8). Figure 7 shows the optimized geometries for the planar

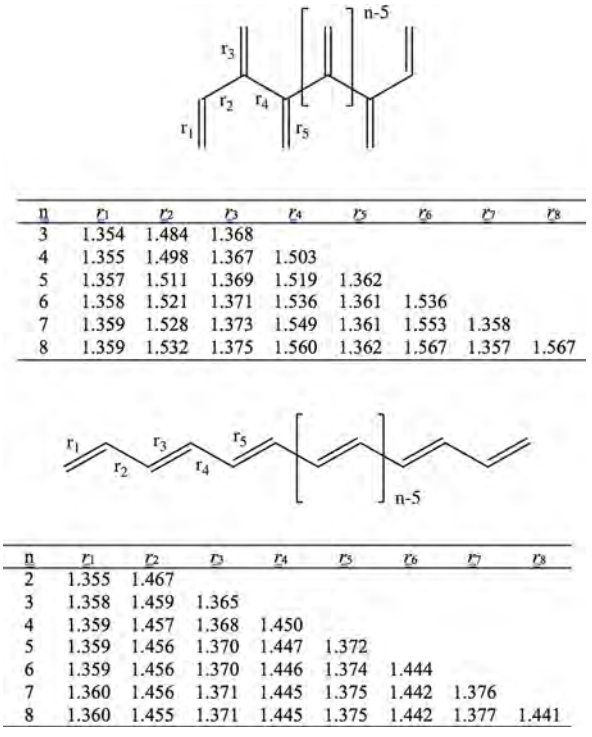

n	r1	r2	r3	r4	r5	r6	r7	r8
3	1.354	1.484	1.368					
4	1.355	1.498	1.367	1.503				
5	1.357	1.511	1.369	1.519	1.362			
6	1.358	1.521	1.371	1.536	1.361	1.536		
7	1.359	1.528	1.373	1.549	1.361	1.553	1.358	
8	1.359	1.532	1.375	1.560	1.362	1.567	1.357	1.567

n	r1	r2	r3	r4	r5	r6	r7	r8
2	1.355	1.467						
3	1.358	1.459	1.365					
4	1.359	1.457	1.368	1.450				
5	1.359	1.456	1.370	1.447	1.372			
6	1.359	1.456	1.370	1.446	1.374	1.444		
7	1.360	1.456	1.371	1.445	1.375	1.442	1.376	
8	1.360	1.455	1.371	1.445	1.375	1.442	1.377	1.441

Figure 7. B3LYP/D95V optimized geometries for $C_{2n}H_{2n+2}$ dendralenes (top) and linear polyenes (bottom).

dendralenes and linear polyenes, having 6−16 carbon atoms. On a quick glance, it is possible to see that dendralenes have a stronger bond alternation; the C═C bonds of the dendralenes are somewhat shorter, while their C−C bonds are significantly longer. These trends indicate, in turn, that the cross-conjugated topology of the dendralenes results in a lesser extent of delocalization compared to the linearly conjugated polyenes. Furthermore, one can observe that these trends become slightly more pronounced as the chain length increases; especially for the [n]dendralenes, the extent of bond alternation increases throughout the series.

Total π-Energies of [n]Dendralenes. The spin-alternant determinant, so-called quasiclassical (QC) state,[74] represents a convenient reference state for quantifying the total π-energy of a state (E_π) or of an individual VB structure. Chart 2 depicts the QC states for hexatriene as a typical representative of linear polyenes and for [3]dendralene as a typical [n]dendralene. It is seen that the spins alternate in both QC states, but the spins are not coupled. As a result, the energy of the QC state is nonbonded and can be used as a reference nonbonded state for determining the π-energy of the desired state.

Table 1 shows the π-energies of the corresponding fundamental Rumer structures of these molecules, as $E_{\pi,0} = E_{QC} - E_{R(0)}$, $C_{2n}H_{2n+2}$ molecules where n = 3−8. Clearly, the cross-conjugated $R(0)$ Rumer structures invariably have higher π-energies compared with the linear isomers. Higher

DOI: 10.1021/jacs.9b01420
J. Am. Chem. Soc. 2019, 141, 6030−6047

Chart 2. QC States for Typical Linear (Left) and Cross-Conjugated (Right) Polyenes

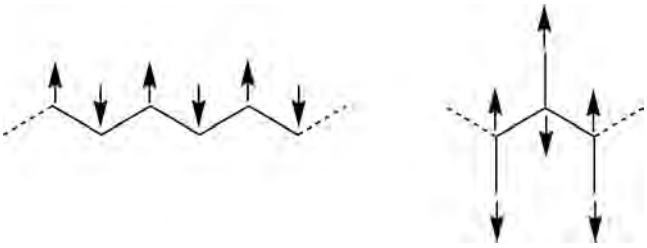

Table 1. VBSCF(BDO-C)/STO-6G and VBSCF(BDO-C)/D95V π-Energies ($E_{\pi,0}$ in kcal mol^{-1}) of Cross-Conjugated [n]Dendralenes and Linearly Conjugated Polyenes $C_{2n}H_{2n+2}$

	$E_{\pi,0}$[a]	
structure	cross-conjugated (STO-6G/D95V)	linearly conjugated (STO-6G/D95V)
C_6H_8	72.4/55.3	71.5/54.4
C_8H_{10}	95.8/73.2	93.1/70.4
$C_{10}H_{12}$	119.7/91.6	114.6/86.2
$C_{12}H_{14}$	143.9/110.4	135.9/101.9
$C_{14}H_{16}$	168.5/129.3	157.1/117.5
$C_{16}H_{18}$	193.1/148.4	178.2/133.0

[a] $E_{\pi,0} = E(\mathrm{QC}) - E(R(0))$.

energy means that the Rumer structure is more stabilized by π-bonding. This in turn reflects the observation made, based on Figure 7, that the cross-conjugated molecules have by and large slightly shorter C═C bonds and longer C−C bonds, compared with the linear isomers. As such, the intrinsic π-bond in C═C is stronger, and at the same time, the π-Pauli repulsion across C−C is weaker for the cross-conjugated molecules compared to their linear isomers. This means essentially that the cross-conjugated isomers are more localized in nature.

Table 2 shows the total π-bond energies, as $E_{\pi,\mathrm{full}} = E_{\mathrm{QC}} - E_{\mathrm{VB,full}}$, for a few members of the two families. The total VBSCF energy involves all the Rumer structures for the two sets of molecules. It is seen that now the linear polyenes are more strongly bonded by the π-electrons compared with the cross-conjugated polyenes. It is clear from Tables 1 and 2 that once we turn on the mixing of the Rumer structures, the π-electronic component gets stabilized by delocalization energy (relative to $R(0)$), and the trend is reversed, in favor of the linear polyenes. As such, the delocalization energies of linear polyenes are larger in absolute magnitude than those of the cross-conjugated polyenes; the difference increases as the polyenes grow (vide infra).

Table 2. VBSCF(BDO-C)/STO-6G and VBSCF(BDO-C)/D95V π-Energies ($E_{\pi,\mathrm{full}}$ in kcal mol^{-1}) of Cross-Conjugated [n]Dendralenes and Linearly Conjugated Polyenes $C_{2n}H_{2n+2}$

	$E_{\pi,\mathrm{full}}$[a]	
structure	cross-conjugated (STO-6G/D95V)	linearly conjugated (STO-6G/D95V)
C_6H_8	83.8/67.0	84.6/68.0
C_8H_{10}	111.8/90.4	114.5/93.3
$C_{10}H_{12}$	140.0/113.4	144.4/118.4
$C_{12}H_{14}$	167.8/137.1	174.5/144.7

[a] $E_{\pi,\mathrm{full}} = E_{\mathrm{QC}} - E_{\mathrm{VB,full}}$.

One can obtain directly the delocalization energy (ΔE_{del}) due to the π-electrons by calculating the full π-space wave function relative to the fundamental Rumer structure, $R(0)$. This requires calculations of the full VB space which can be done in the following two ways:

(a) The CASSCF(full π-valence) wave function is in principle "identical" to VBSCF with the full sets of Rumer structures and of the ionic structures. As such, using CASSCF(full π-valence) instead of VBSCF(BDO-C) to calculate the fully delocalized π-valence state will provide upper-bound values of the delocalization energy (with the exception of dynamic correlation effects) for the full π-active space. This upper bound value of the delocalization energy is defined in eq 4:

$$\Delta E_{\text{del-CASSCF(full-}\pi\text{)}} = E_{R(0)} - E_{\text{CASSCF(full-}\pi\text{)}} \quad (4)$$

(b) Alternatively, the full π-valence state can be calculated using the full Rumer basis set; hence,

$$\Delta E_{\text{del-VBSCF(BDO-C)}} = E_{R(0)} - E_{\mathrm{VB,full}} \quad (5)$$

Using VBSCF with BDOs limits us to C_6H_8−$C_{12}H_{14}$ because the optimization of all the BDOs in all the Rumer structures is rather time-consuming. However, as we have already shown[7] and is further demonstrated here (cf. Table S21), the VBSCF wave function, which uses in addition to $R(0)$, only the Rumer structures of the first block that involve only one long-bond, VBSCF(BDO-C; $R(0) + R(1,j)$) lead to total energies and other properties almost identical to those obtained from VBSCF-(BDO-C; full π-valence). Thus, eq 5, becomes eq 6:

$$\Delta E_{\text{del-VBSCF(BDO-C)}} = E_{R(0)} - E_{\mathrm{VB},R(0)+R(1,j)} \quad (6)$$

The ΔE_{del} values for both the linear and cross-conjugated polyenes, calculated according to eqs 4−6, have been summarized in the Supporting Information (section S5). From these data, one can conclude that the basis set (STO-6G vs D95V) makes a rather small difference, with slightly higher $\Delta E_{\mathrm{del,vbscf}}$ values for D95V, and that the evaluation of $\Delta E_{\text{del-casscf}}$ using CASSCF leads to higher delocalization energies than the VBSCF(BDO-C) method.

In order to extract a clear trend in the evolution of the delocalization energy with an increasing chain length, we present the values for the delocalization energy per C═C bond, $\Delta E_{\mathrm{del}}/n$ in Tables 3 and 4. For $\Delta E_{\text{del-VBSCF(BDO-C)}}/n$, we only show the values for the first Rumer block, $R(1,j)$.

From Tables 3 and 4, it can be concluded that the linear and cross-conjugated compounds exhibit dissimilar trends in the evolutions of their delocalization energy as the chains become longer. For linear polyenes, we see that $\Delta E_{\mathrm{del}}/n$ increases steadily and converges as n becomes larger, and, as already

Table 3. $\Delta E_{\text{del-CASSCF}}/n$ in kcal mol^{-1} for Linear and Cross-Conjugated Polyenes $C_{2n}H_{2n+2}$ in the STO-6G and D95V Basis Sets

	$\Delta E_{\text{del-CASSCF}}(\text{full-}\pi)/n$	
structure	cross-conjugated (STO-6G/D95V)	linearly conjugated (STO-6G/D95V)
C_6H_8	6.1/6.4	7.0/7.2
C_8H_{10}	6.5/6.8	8.3/8.5
$C_{10}H_{12}$	6.4/6.9	9.1/9.3
$C_{12}H_{14}$	6.4/6.8	9.7/9.8
$C_{14}H_{16}$	6.3/6.7	10.2/10.3
$C_{16}H_{18}$	6.1/6.6	10.5/10.6

DOI: 10.1021/jacs.9b01420
J. Am. Chem. Soc. 2019, 141, 6030−6047

Table 4. $\Delta E_{\text{del-VBSCF(BDO-C)}}/n$,[a] in kcal mol^{-1}, for Linear and Cross-Conjugated Polyenes $C_{2n}H_{2n+2}$ in the STO-6G and D95V Basis Sets

	$\Delta E_{\text{del-VBSCF}}$(full-$\pi$)/$n$	
structure	cross-conjugated (STO-6G/D95V)	linearly conjugated (STO-6G/D95V)
C_6H_8	3.7/3.7	4.5/4.4
C_8H_{10}	3.8/3.8	5.2/5.2
$C_{10}H_{12}$	3.7/3.8	5.6/5.7
$C_{12}H_{14}$	3.6/3.7	5.9/5.9
$C_{14}H_{16}$	3.6/3.6	6.0/6.1
$C_{16}H_{18}$	3.3/3.4	6.1/--
$C_{18}H_{20}$	3.2/3.3	6.1/--

[a] $\Delta E_{\text{del-VBSCF(BDO-C)}}/n = (E(R(0)) - E(R(0) + R(1,j)))/n$.

established in our previous work, this increase in $\Delta E_{\text{del}}/n$, as n increases, for the linear polyenes levels off at around 6 kcal/mol at the VBSCF level of theory and at 11 kcal/mol at the CASSCF level of theory. For the cross-conjugated polyenes on the other hand, $\Delta E_{\text{del}}/n$ remains more or less constant with increasing n throughout the entire series and even goes down slightly. This very slow decrease in $\Delta E_{\text{del}}/n$ as n increases can presumably be attributed to structural effects; as pointed out before, as the chain length of the dendralene increases, the extent of bond alternation increases ever so slightly throughout the entire chain, indicating an increasing localization (especially in the formal C−C single bonds, which get longer). We were unable to determine whether this localization effect in dendralenes persists much further as the chain length increases or dies out very fast due to the limitations of our computational facilities. As such, we cannot accurately project a limiting value for $\Delta E_{\text{del}}/n$ as n goes to infinity, but we can reasonably expect that this value should lie somewhere in the range between 1.5 and 3 kcal/mol at VBSCF level of theory and 4−6 kcal/mol at CASSCF level of theory. Nevertheless, given that the slight decrease in $\Delta E_{\text{del}}/n$ is presumably caused by a structural effect spread out over the entire molecule, we can confidently conclude that every unit added to a dendralene-chain leads *to an intrinsically constant and small contribution to* ΔE_{del}.

Given the estimated limiting values for $\Delta E_{\text{del}}/n$ mentioned in the previous paragraph, we can expect that, as n goes to infinity, the delocalization energy per C═C bond of the infinitely long linear polyene would be approximately 4−6 kcal/mol larger than that of the corresponding cross-conjugated polyenes. This is the lower limit estimate of the difference, since the planar model for dendralene overestimates the ΔE_{del} quantity anyway.

Trends in the VB Wave Functions of Cross-Conjugated and Linearly Conjugated Polyenes. Yet another way of probing the different delocalization patterns of the two polyene families is to consider the variation of the corresponding VBSCF wave functions in terms of their Rumer structural constituents (see Figures 3 and 4). Table 5 collects the weights of the Rumer structures (W) for the fundamental structure, $R(0)$, and the collective structures $R(1,j)$ that possess a single long-bond.

One feature that stands out is the decay of the weight of the fundamental structure with the increased polyene size (n). It is seen that while for the linear series, $W(R(0))$ decreases from 0.758 to 0.364, the corresponding weight for the cross-conjugated series decays moderately, from 0.777 to 0.596. At the same time, in both series, the combined weight of all the Rumer structures that possess a single long-bond, $W(R(1))$, increases. However, while this increase is fast for the linear

Table 5. Weights[a] of the Fundamental Rumer Structures $W(R(0))$ and the Corresponding Blocks with a Single Long-Bond, $W(R(1))$, in Cross-Conjugated vs Linear Polyenes $C_{2n}H_{2n+2}$

	cross-conjugated		linear	
	$W(R(0))$	$W(R(1))$[b]	$W(R(0))$	$W(R(1))$[b]
C_6H_8	0.777	0.205	0.758	0.250
C_8H_{10}	0.704	0.286	0.588	0.356
$C_{10}H_{12}$	0.637	0.351	0.473	0.453
$C_{12}H_{14}$	0.596	0.350	0.364	0.508

[a] Weights calculated at the VBSCF(BDO-C)/D95V level of theory. [b] $W(R(1))$ is the collective weight of all the $R(1,j)$ Rumer structures.

polyenes, 0.250 → 0.508, in the cross-conjugated series the increase is moderate, 0.205→ 0.350, and beyond C_{10} the value seems to remain constant (0.35).

An increase of $W(R(1))$ means more mixing of these "excited" Rumer structures into the fundamental one ($R(0)$). This is in perfect harmony with all previous conclusions that the cross-conjugated polyenes are endowed with a reduced delocalization, compared with the linear polyenes. In fact, one can see from Table 5, that in the linear series, the pack of $R(1,j)$ Rumer structures has a collective weight larger than that of $R(0)$ already for $C_{12}H_{14}$, as found previously.[7] The linear polyene becomes quickly a pack of shifting long-bond diradicaloid structures, whereas the cross-conjugated polyene remains close to the original fundamental structure. Impeded delocalization in cross-conjugation emerges clearly from all the above probes.

3.3. Comparison of Linear- and Cross-Conjugated Polyenes to Quinodimethanes. Before proceeding to the Discussion section, it is interesting to compare our two series of polyenes to *o*-quinodimethnes (*o*-QDM), **3** (Chart 1) and to *p*-quinodimethanes (*p*-QDM), **4**. The QDM hydrocarbons have formally two polyenes chains that are cross-conjugated, and their comparison to the linear and cross-conjugated polyenes may be instructive. Since the number of electrons in the QDM molecules increases rapidly from the smaller members C_8H_8 to larger ones, the VB treatment was restricted to two to three members of this series of molecules, just enough to establish comparison with the linear polyenes and dendralenes.

Delocalization in QDM. A test of the HOMO−LUMO gaps (Table S22), $\Delta E_{\text{HOMO−LUMO}}$, shows that the corresponding values vary in the following order: $\Delta E_{\text{HOMO−LUMO}}$(*o*-QDM) < $\Delta E_{\text{HOMO−LUMO}}$(*p*-QDM) < $\Delta E_{\text{HOMO−LUMO}}$(linear polyenes) ≪ $\Delta E_{\text{HOMO−LUMO}}$(dendralene). The corresponding ΔE_{ST} values for the QDM molecules (Tables S23−S25) are summarized in Figure 8.

Even though the quantitative ΔE_{ST} values presented in Figure 8 exhibit a significant dependence on the method used, one can observe that the calculated excitation energies unequivocally follow the same pattern as the corresponding HOMO−LUMO gaps; the values for the QDM molecules are smaller than those for the linear polyenes, and the latter compounds have values much smaller than those for the cross-conjugated polyenes. Furthermore, our B3LYP calculations indicate that already for *o*-$C_{16}H_{12}$ and *p*-$C_{20}H_{16}$ the solutions for the singlet ground states show an instability to spin symmetry breaking (cf. Table S24), indicating significant electron correlation and diradicaloid natures. The computational challenges posed by the growing diradical character upon elongation of these compounds offer an explanation for the difficulty to obtain unequivocal quantitative values using the standard methods employed above. For a more

DOI: 10.1021/jacs.9b01420
J. Am. Chem. Soc. 2019, 141, 6030−6047

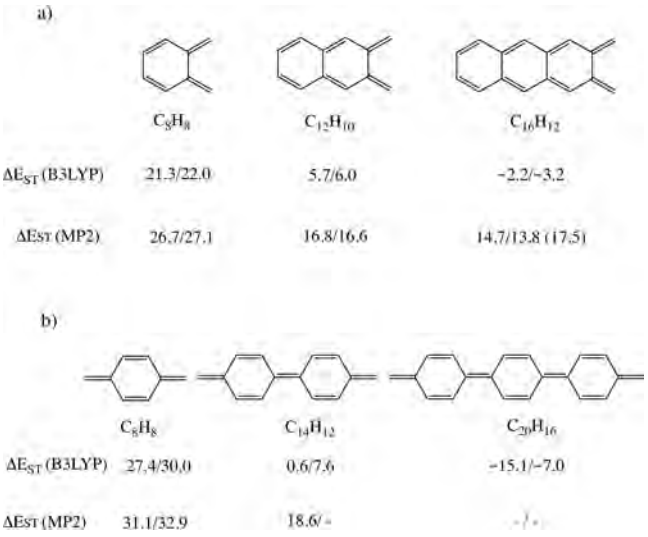

Figure 8. (Adiabatic) Singlet-to-triplet excitation energies, ΔE_{ST} (in kcal/mol), calculated at B3LYP and MP2 levels of theory: (a) C_8H_8, $C_{12}H_{10}$, and $C_{16}H_{12}$ *o*-QDM molecules. (b) C_8H_8, $C_{14}H_{12}$, and $C_{20}H_{16}$ *p*-QDM molecules. The values are given in the following order of basis sets, STO-6G/D95V. The datum in parentheses in part a is calculated by VBSCF. As demonstrated in Table S27 in the Supporting Information, the DFT results are essentially functional independent. We also note that at MP2 level of theory, a fragmentation of the singlet state of $C_{20}H_{16}$ was observed so that no ΔE_{ST} value could be obtained.

in-depth discussion, we refer to the work by Malrieu and coworkers.[80,81]

As such, both quantities, $\Delta E_{HOMO-LUMO}$ and ΔE_{ST}, indicate the QDM molecules are more delocalized and have a higher diradicaloid character compared with the linear polyenes. Since the *o*-QDM π-systems (**3** in Chart 1) involves two cross-conjugated *s-transoid* chains, it follows that the cross-conjugation in the double-chain augments the delocalization and diradicaloid character in the *o*-QDM series. Similarly, the delocalization of the *s-transoid,cisoid* chain of *p*-QDM is intensified by capping the *cisoid* parts.

VBSCF(BDO-C)/D95V weights for all the molecular systems collected in Table 6 confirm this conclusion. It is seen

Table 6. Weights of Rumer Structures for Linear- and Cross-Conjugated Polyenes ($C_{2n}H_{2n+2}$), *o*-QDM Molecules ($C_{2n}H_{n+4}$), and the Smallest *p*-QDM (C_8H_8)

	$W(R(0))/W(R(1))$ Values, VBSCF(BDO-C)/D95V			
n	linear	cross-conjugated	*o*-QDM	*p*-QDM
3	0.758/0.250[a]	0.777/0.205		
4	0.588/0.356	0.704/0.286	0.529/0.444	
4[b]				0.579/0.393[b]
5	0.473/0.453	0.637/0.351		
6	0.364/0.508	0.596/0.350	0.222/0.557	

[a] $W(R(2)) = -0.008$. [b] *p*-QDM C_8H_8

that the $W(R(0))$ weight of the fundamental Lewis structure for *o*-QDM molecule decays faster than in the linear polyenes, and at $C_{12}H_{10}$, the *o*-QDM becomes a set of shifting 1,*m*-diradicals, in a more pronounced manner than the $C_{12}H_{14}$ linear polyene. For *p*-QDM, $W(R(0))$ is available only for the smallest species C_8H_8 and is already smaller than the corresponding value for the linear C_8H_{10} polyene, indicating its fast conversion to a 1,*m*-diradicaloid. The dendralenes display the largest $W(R(0))$ values, which decay slowly.

The above conclusions are supported by the delocalization energies, $\Delta E_{del\text{-}CASSCF}$, in Table 7. Clearly, the QDM molecules have the most efficient delocalization of either one of the polyene families considered here (section VII in the Supporting Information).

Table 7. $\Delta E_{del,CASSCF}$ Values (in kcal/mol) for Linear- and Cross-Conjugated Polyenes ($C_{2n}H_{2n+2}$), *o*-QDM molecules ($C_{2n}H_{n+4}$), and *p*-QDM Molecules (C_8H_8, $C_{14}H_{12}$)

	$\Delta E_{del,CASSCF/D95V}$			
n	linear	cross-conjugated	*o*-QDM	*p*-QDM
3	21.6	19.2		
4	33.8	27.4	41.1	42.3
6	59.0	41.0	79.8	
7	71.9	46.9		96.1
8	84.5	52.5	122.7	

4. DISCUSSION

The above results show that in any way we look at the various "polyenes", the [*n*]dendralenes are the least efficient in promoting delocalization between the double bonds of the fundamental Rumer structure, $R(0)$. The linear polyenes are rather effective in this sense, while the *o*- and *p*-QDM molecules seem to do so the most efficiently among the molecular types we examined here. Our goal in this section is to try to comprehend and model the weak conjugation of the dendralenes vs linear polyenes. Subsequently, we shall provide complementary insight on the manner by which the Rumer structures favor/disfavor electron transmission in linear polyenes and QDMs while inhibiting it (sealing it off) in cross-conjugated ones.

4.1. What Are the Factors That Govern ΔE_{del}? A perturbation−theoretic[74,82] treatment of the mixing of the "excited" Rumer structures, $R(I,j)$, into the fundamental one, $R(0)$, provides the means to conceptualize the behavior of ΔE_{del}. Figure 9 shows a schematic VB-mixing diagram, in which the

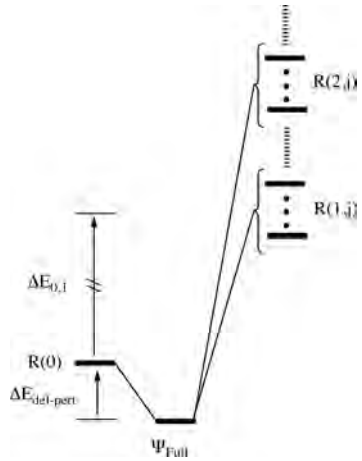

Figure 9. VB mixing diagram between $R(0)$ and the components of the excited Rumer structures in various blocks, symbolized collectively as $R(I,j)$, where I is the block number ($I = 1, 2, ...$) while j is the number of the Rumer structure within its specific block. The energy gap $\Delta E_{0,1}$ between $R(0)$ and the first block $R(1)$ is indicated specifically in the diagram.

DOI: 10.1021/jacs.9b01420
J. Am. Chem. Soc. 2019, 141, 6030−6047

excited Rumer structures mix into $R(0)$ and generate the full state, Ψ_{full}, which is lowered in energy relative to $R(0)$ by the quantity, $\Delta E_{del\text{-}pert}$. The $\Delta E_{del\text{-}pert}$ quantity is in turn a sum of the individual contributions of the excited Rumer structures, $R(I,j)$.

As shown previously, the mixing of a given excited Rumer j in any given block is expressed as

$$\Delta E_{del,j} = C_j \beta_{0,j} \tag{7}$$

Here, C_j is the coefficient of the particular excited Rumer structure, and $\beta_{0,j}$ is the corresponding reduced matrix element[7,83] for $R(0)$ and $R(I,j)$. The total ΔE_{del} quantity is a summation of all the terms.

Table 8 collects the VBSCF computed ΔE_{del} values alongside the $\Delta E_{del\text{-}Pert}$ quantities evaluated by mixing the various $R(I,j)$

Table 8. Delocalization Energy Values $\Delta E_{del\text{-}VBSCF}$ and Perturbationally Estimated $\Delta E_{del,pert}$ Values for Linear and Cross-Conjugated Systems and QDMs[a]

	STO-6G/BDO		D95V/BDO	
	$\Delta E_{del\text{-}vbscf}$	$\Delta E_{del\text{-}Pert}$	$\Delta E_{del\text{-}vbscf}$	$\Delta E_{del\text{-}Pert}$
C_6H_8 (linear)	13.1	13.1	13.7	13.5
C_8H_{10} (linear)	21.3	20.7	22.9	22.8
$C_{10}H_{12}$ (linear)	29.8	28.5	32.2	32.4
$C_{12}H_{14}$ (linear)	38.7	36.0	42.8	45.0
C_6H_8 (cross)	11.4	11.4	11.8	11.4
C_8H_{10} (cross)	16.0	16.2	17.2	17.2
$C_{10}H_{12}$ (cross)	20.3	20.1	21.8	22.3
$C_{12}H_{14}$ (cross)	23.9	23.5	26.7	28.1
C_8H_8 (*o*-QDM)	25.1	24.8	26.9	26.7
$C_{12}H_{10}$ (*o*-QDM)	51.0	44.3	58.2	62.2
C_8H_8 (*p*-QDM)	25.7	24.8	27.1	26.7

[a]All energies are in kcal/mol. $\Delta E_{del\text{-}Pert}$ includes all the excited Rumer structures.

Rumer structures into $R(0)$, as depicted in Figure 9. It is seen that the delocalization energy calculated by the perturbation expression in eq 7 leads to values very close to the corresponding full-VBSCF values. The largest deviations ($\lesssim$5%) are for $C_{12}H_{10}$ *o*-QDM. Furthermore, the perturbation treatment picks up the trend that ΔE_{del}(cross-conjugated) $\ll \Delta E_{del}$(linear) $< \Delta E_{del}$(*p*-QDM) $\sim \Delta E_{del}$(*o*-QDM).

For qualitative purposes, we do not have to go so far. As we demonstrated previously[7] and here as well (cf. Table S21), the VBSCF energy of a wave function made of $R(0)$ and the Rumer structures of block 1, $R(1,j)$, is very close to the full VBSCF energy, including the entire ensemble of Rumer structures. Using eq 7, one can see that the above trends are determined by (a) the number of Rumer structures in the $R(1)$ block, (b) the corresponding reduced matrix elements, $\beta_{0,j}$, and (c) the mixing coefficients C_j; the latter depend on both the reduced matrix element and the energy gaps relative to $R(0)$.

To conceptualize the $\Delta E_{del\text{-}Pert}$ trends for the various systems, we focus on the C_8 molecules that possess the same number of double bonds (four) in all the above conjugative topologies. Figure 10 shows these $R(0)$ and $R(1,j)$ Rumer sets for the C_8 molecule for the various conjugation topologies, and it is seen that the cross-conjugated C_8H_{10} has only three $R(1)$ structures, while the linear congener has six. Similarly, the *o*,*p*-QDM C8 molecules have seven and six $R(1)$ structures, respectively (sections VIII and IX).

It is seen that the C_8 dendralene has three $R(1)$ Rumer structures, wherein the delocalization branches between two pathways; one is perpendicular to the C−C backbone and within the consecutive butadieneic units, and the second is across the C−C backbone. In contrast, in the other C_8 molecules there are at least twice as many Rumer structures in $R(1)$, where the long-bond is delocalized, reaching from one end of the molecule to the other. Thus, the small member C_8 already shows that the dendralene is "least delocalized" among the four conjugation topologies.

This pattern is quite general: the number of $R(1,j)$ structures d_1 as a function of n, the number of double bonds in the conjugated system, follows from eqs 8 and 9, for linear polyenes (eq 8) and cross-conjugated (eq 9). The expressions for the QDM molecules are more complex, and their derivation is shown in the Supporting Information (Appendix 3). Thus, the number d_1 of $R(1)$ block structures for *o*-QDM increases to 20 for C_{12}, then to 42 for C_{16}, all the way to 182 for C_{28}, whereas for *p*-QDM d_1 shoots up faster, 28 for C_{14}, 82 for C_{20}, and all the way to 668 for C_{32}. By comparison, for the C_{12}−C_{32} linear polyenes the d_1 ranges from 15 to 496. Since the total number of Rumer structures is constant for a given n, this means that in the QDM topologies the branched conjugation makes many Rumer structures belonging to $R(1)$ rather than to the higher energy blocks.

$$d_1 = \binom{n}{2} \tag{8}$$

$$d_1 = n - 1 \tag{9}$$

It is apparent that the cross-conjugated dendralenes will have as a rule the smallest number of $R(1,j)$ structures, compared to linear polyenes, whereas the QDM molecules will possess much larger number of Rumer structures in the respective $R(1)$ blocks (see Tables S40, S41, and A3.4 in the Supporting Information). If we assume for simplicity that all the $R(1,j)$ structures mix to the same extent into $R(0)$, we can predict that the ΔE_{del} quantity will vary linearly with the number of $R(1,j)$ structures, d_1. Figure 11a and Figure 11b show precisely this behavior for dendralenes and linear polyenes. It is seen that both $\Delta E_{del\text{-}Pert}$ and $\Delta E_{del\text{-}vbscf}$ quantities vary linearly with d_1, for C_6H_8−$C_{12}H_{14}$, and that the dendralenes have poor delocalization compared with their linear isomers.

The circles and pentagons in Figure 11b are the corresponding $\Delta E_{del\text{-}Pert}$ (blue and green, respectively) and $\Delta E_{del\text{-}VBSCF}$ (magenta and yellow, respectively) for the QDM molecules. It is apparent that the conjugation topology of these two molecules is more efficient than that in the linear polyenes of the same number of double bonds. The detailed analysis of the C_8 molecules provides some insight into this trend. Thus, while in cross-conjugated C_8, there are three Rumer structures which together contribute ~15 kcal/mol to $\Delta E_{del\text{-}pert}$; in the linear C_8 polyenes there are, in addition to the three shorter range 1,4-bond $R(1)$ structures, also three $R(1)$ structures with long-range bonding (1,6 and 1,8), which together contribute ~20 kcal/mol. In *p*- and *o*-QDM C_8, the Rumer structures with the long-range bonds contribute even more, thus reaching ~23 and ~22 kcal/mol, respectively. This difference between the various conjugation modes will increase as the size of the molecules increases: the split delocalization of the dendralenes to the butadienic branches with a smaller contribution along the C−C backbone path (Tables 3 and 4 and discussions thereof) will lag behind the contiguous delocalization in the linear polyenes and

DOI: 10.1021/jacs.9b01420
J. Am. Chem. Soc. 2019, 141, 6030−6047

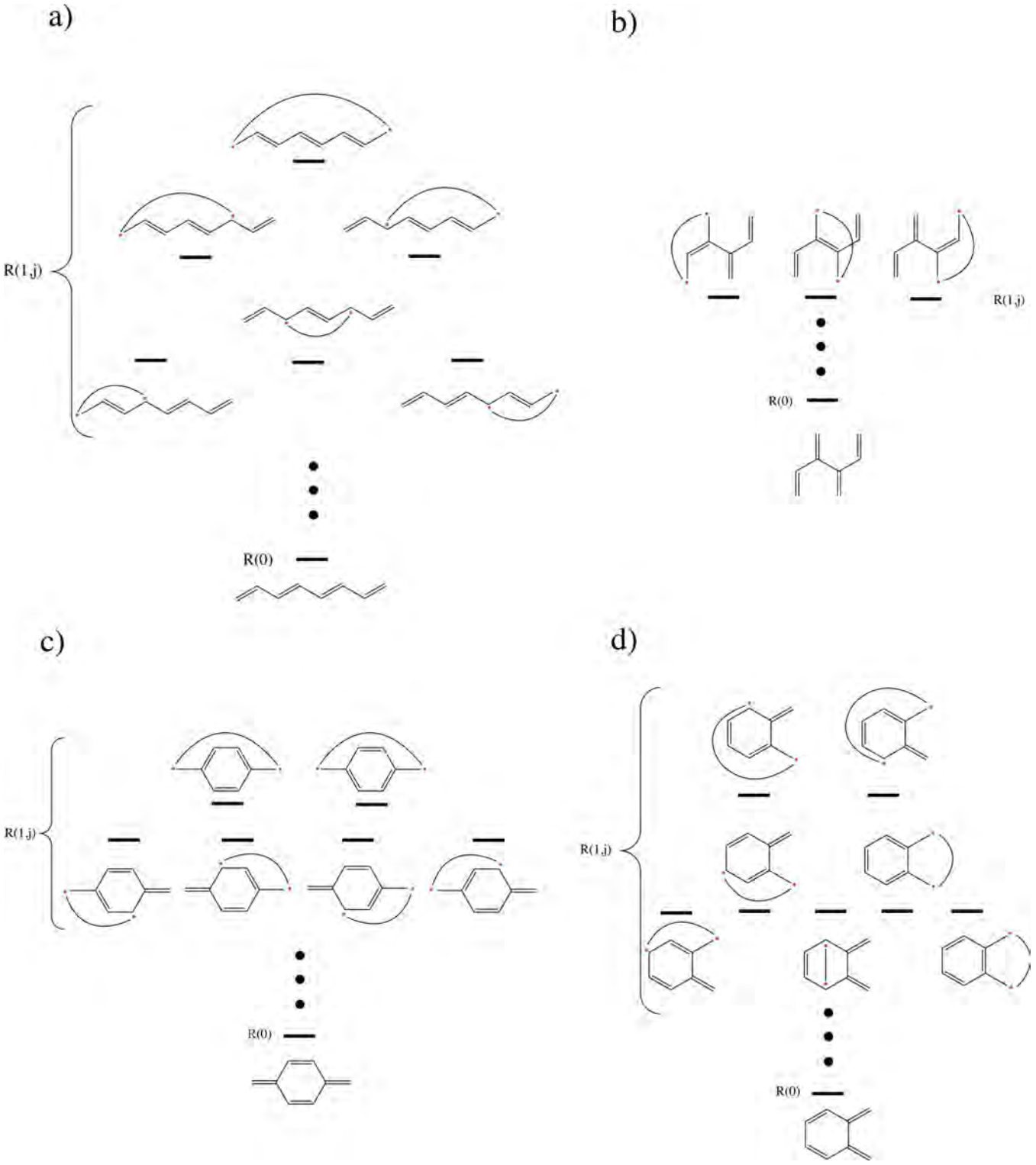

Figure 10. Fundamental Rumer structure, $R(0)$, and the ones in the first excited block $R(1,j)$, in C_8 molecules of the (a) linear polyene, (b) cross-conjugated polyene, (c) *p*-QDM, and (d) *o*-QDM.

the QDM molecules. Furthermore, in the actual geometries of the cross-conjugated polyenes, the butadiene units undergo twisting around the intervening C−C bonds such that the delocalization via the C−C backbone path will be further turned off.

4.2. The Decay of the Weight of the Fundamental Rumer Structures with the Growing Size of the Conjugated System.

As we saw all along, the conjugation in $C_{2n}H_{2n+2}$ dendralenes is severely impeded compared with their linear isomers. In addition to the ΔE_{del} properties, this is expressed also in the wave function (Table 6), wherein the weights of the fundamental Rumer structure, $W(R(0))$, decay fast in linear polyene ($C_{2n}H_{2n+2}$) but slowly in dendralenes, as n grows larger. As we showed above and before,[7] a linear polyene

DOI: 10.1021/jacs.9b01420
J. Am. Chem. Soc. 2019, 141, 6030−6047

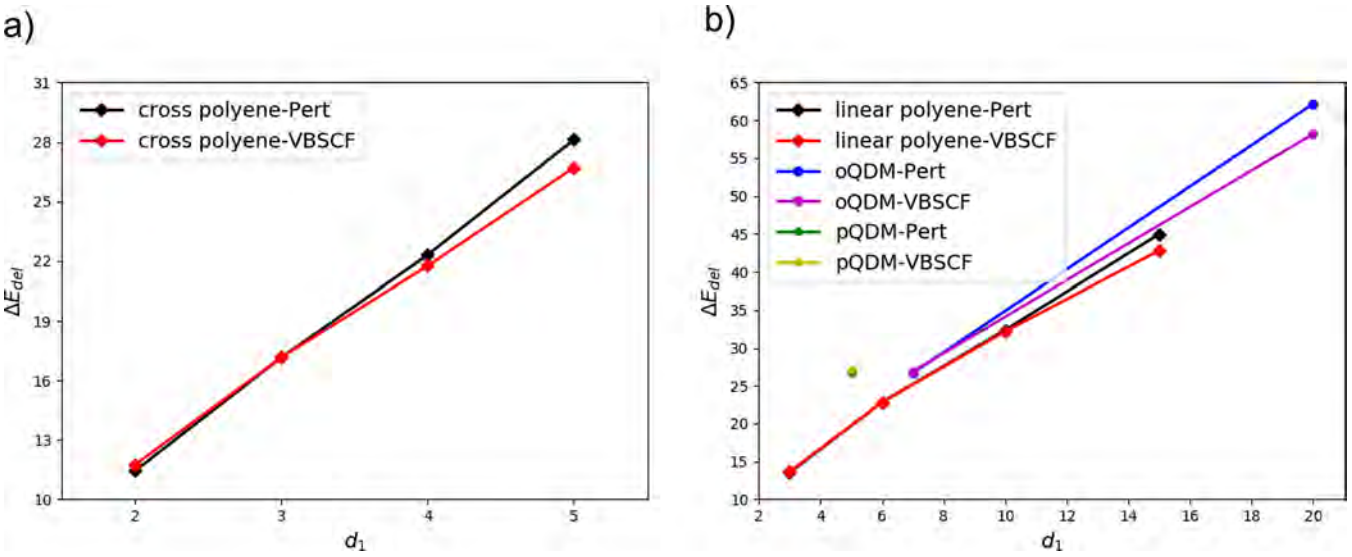

Figure 11. $\Delta E_{\text{del-pert}}$ (black diamonds) and $\Delta E_{\text{del,vbscf}}$ (red diamonds) values calculated at VBSCF(BDO)/D95V level plotted against the number (d_1) of Rumer structures in the first excited block ($R(1)$) for (a) cross-conjugated dendralenes and (b) linear polyenes. The circles in part b correspond to the $\Delta E_{\text{del-pert}}$ (blue) and $\Delta E_{\text{del,vbscf}}$ (magenta) for *o*-QDM, and the corresponding green and yellow pentagons correspond to the *p*-QDM C_8H_8.

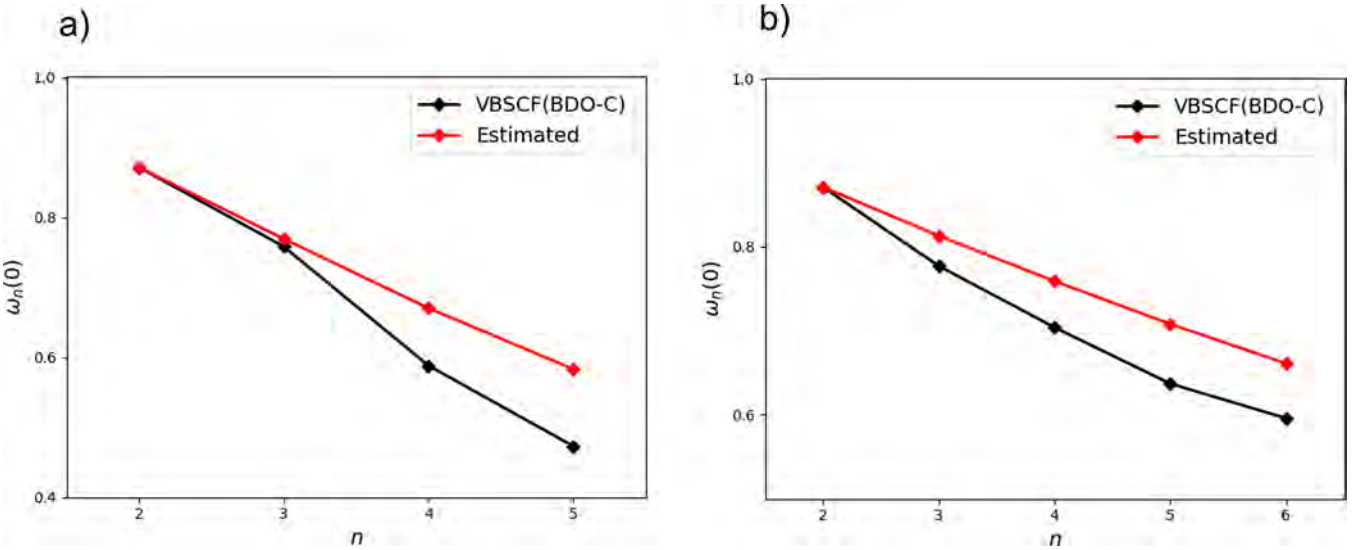

Figure 12. Decay of $W_n(0)$ as a function of n for $C_{2n}H_{2n+2}$: (a) linear polyenes, (b) cross-conjugated dendralenes.

can be viewed as *a shifting 1,m-diradicaloid* ($m \geq 4$), which accounts for the fact that the $R(1,j)$ structures mix efficiently with $R(0)$, using both 1,4 and 1,6 and ..., 1,2n long-bonds. For the dendralenes on the other hand, as we found in the present study, the $R(1,j)$ structures which mix with the corresponding fundamental Rumer structures have only 1,4 long-bonds (e.g., see Figure 10) in the butadienic unit, perpendicular to the C−C backbone. Along the C−C backbone of the dendralenes, the delocalization per C−C unit decreases with the increase in n (Tables 3 and 4) and will be almost negligible in the actual nonplanar geometries.

As such, for the sake of simplicity, we can view the weights of the fundamental structure $W_n(0)$ for $C_{2n}H_{2n+2}$ polyenes (linear or cross-conjugated) as products of the $W_2(0)$ weights (probabilities) of all the butadienic segments, which participate in the main delocalization pathway; in the case of linear polyenes, there are $n-1$ butadienic segments overlapping along the chain (hence allowing for long-bonds of the type 1,4; 1,6; 1,8; ...; 1,2n), while in dendralenes, there are $n/(2-1)$ disjointed butadiene segments perpendicular to the C−C chain. Equations 10 and 11 use this rationale to predict the decay rates for $R(0)$ in the wave function of a linear- and cross-conjugated polyene, $C_{2n}H_{2n+2}$, using $W_2(0) = 0.871$.[7]

$$W_n(0) = [W_2(0)]^{n-1} \qquad \text{linear} \tag{10}$$

$$W_n(0) = [W_2(0)]^{0.5n-1} \qquad \text{cross-conjugated} \tag{11}$$

The results are plotted in Figure 12, using the corresponding $W_n(0)$ obtained from VBSCF(BDO-C) calculations and equations (eqs 10 and 11). It is seen that the simple equations (eqs 10 and 11) predict the decay rate reasonably well. The rate is large in Figure 12a for the linear polyenes and quite tempered in Figure 12b for the dendralenes. Note that the VBSCF(BDO-C) values are always smaller than those of the model equations because the VBSCF calculations take into account the entire

DOI: 10.1021/jacs.9b01420
J. Am. Chem. Soc. 2019, 141, 6030−6047

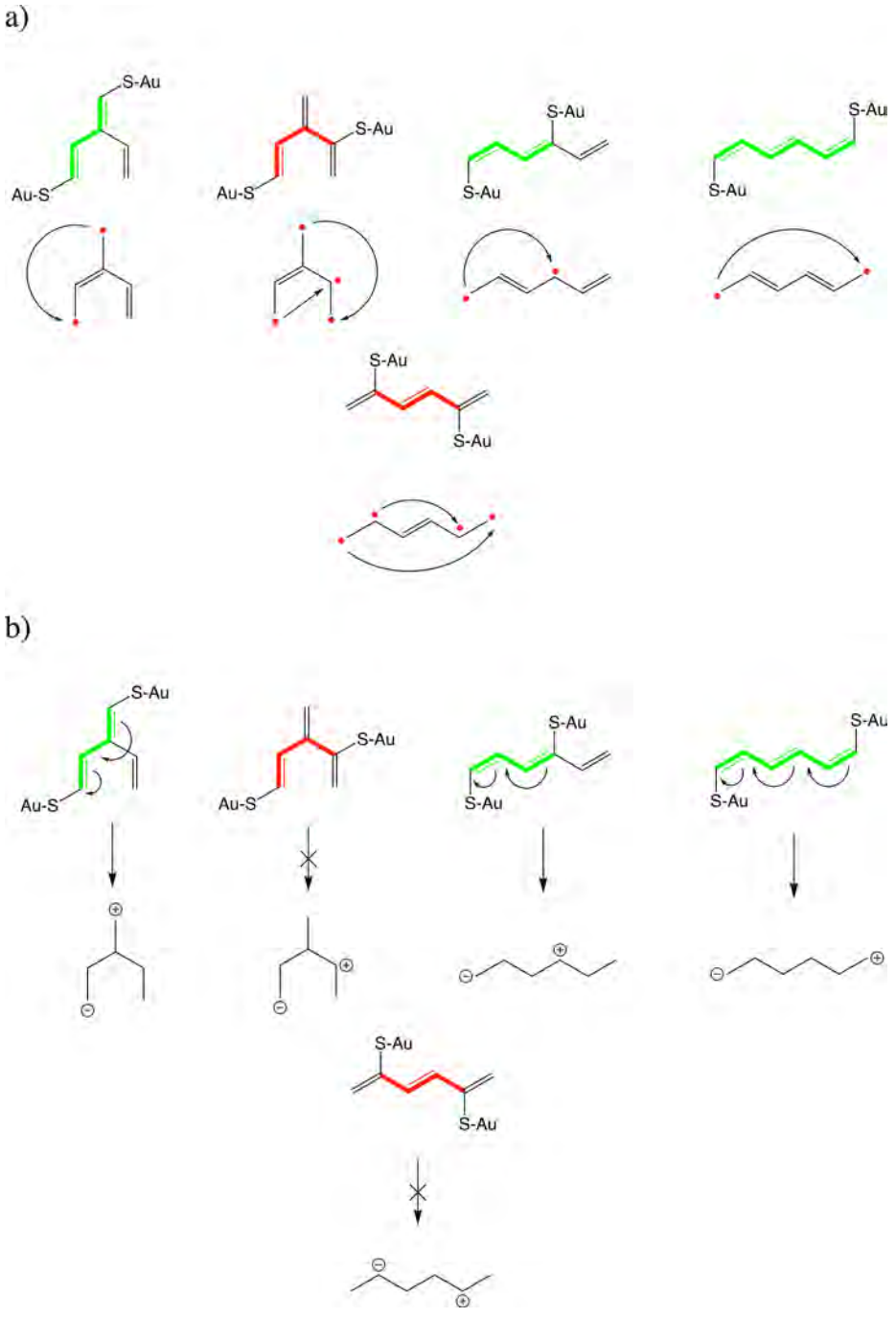

Figure 13. (a) The occurrence of quantum interference in molecular conductance experiments appears to be determined by the presence/absence of "electronic coupling" between the contact sites. If a combination of contact sites corresponds to an $R(1)$ structure, no destructive quantum interference occurs (cf. the green paths). When this is not the case, QI occurs (the red paths). (b) Curly arrow drawings are a handy tool to determine whether two sites in a conjugated system can be connected through a single long-bond, thus indicating whether or not these sites are "electronically coupled". S−Au indicates the electrode attachment site in the transport-measurement experiment, where S is a typical linker atom and Au is a typical electrode element.

VBSCF wave function, wherein higher rank Rumer structures are mixed as well.

The expressions with $W(0)$ for the QDM families are less simple to derive. Therefore, we relegated the discussion of these quantities to the Supporting Information (Appendix 3). However, we know from the foregoing discussions that in both families, the delocalization in the polyenes chains is being augmented either by the second chain in *o*-QDM or by the C═C caps in *p*-QDM. Therefore, a simple way to see what happens to $W(0)$ is to consider the overlapping C8 units. For example, in C12 *o*-QDM, we have two such units, and based on the C8 datum in Table 6, we can predict that $W(0)$ for C12 would be $\sim(0.579)^2 = 0.28$ (vis-à-vis 0.222 computed in Table 6). Similarly, for C14 *p*-QDM we have two overlapping C8 units which lead to $W(0) = (0.579)^2 = 0.34$. While these estimations are quite rough, they nevertheless tell us that in these two families, the molecules become shifting diradicaloids at C12 and C14, respectively.

4.3. Electron Transmission Capabilities of Polyenes and Quinodimethane Conjugated Molecules. As men-

DOI: 10.1021/jacs.9b01420
J. Am. Chem. Soc. 2019, 141, 6030−6047

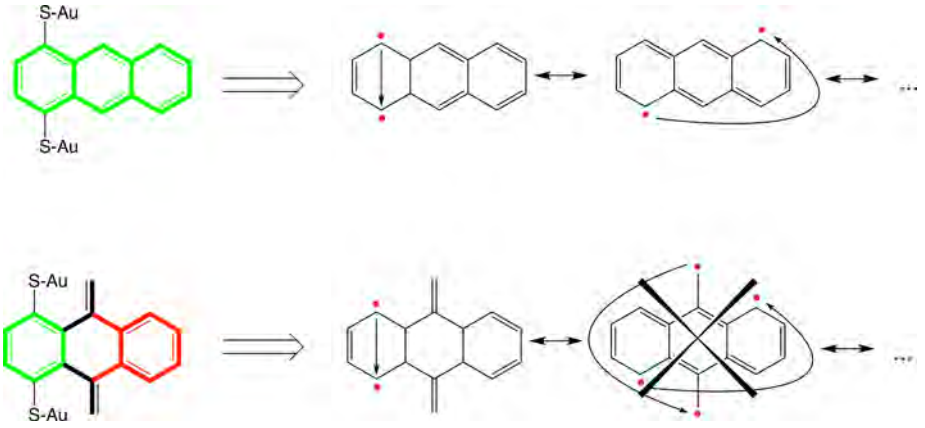

Figure 14. Comparison of anthracene (top) and a cross-conjugated anthracene (bottom). Note that the cross-conjugation feature renders connection of sites on opposite side of the feature in $R(1)$ structures impossible. As such, all electronic couplings between the contact positions and sites beyond the feature are effectively destroyed; i.e., cross-conjugation can be understood to essentially seal-off specific parts of the polyene molecule for delocalization.

tioned in the Introduction of this paper, part of our motivation to take a closer look at the wave function of cross-conjugated compounds has been the apparent connection between the structural motif associated with cross-conjugation and the occurrence of (destructive) quantum interference, i.e., a sharp reduction in the coherent transport of electrons through the molecule in molecular conductance experiments.[8,9,55,56] The results presented above seem to indicate that the origin of this connection can be attributed to whether or not the two contact positions on the molecule lie on the contiguous delocalization path of the molecule and hence are "electronically coupled".

Recall that for all the polyene compounds, considered both here and before,[7] only the fundamental Rumer structure, $R(0)$, and the first block of diradicaloid structures, $R(1)$, played a significant role in the wave function. In linearly conjugated compounds, a long-bond in $R(1)$ can stretch across the main conjugation path unhindered, resulting in the presence of 1,*m*-diradical structures in the wave function ($m = 4, ..., 2n$). As such, electronic delocalization between any two sites corresponding to the couple of radicaloid sites in one of the $R(1)$ structures is significant. Accordingly, one observes no quantum interference in molecular conductance measurements when contacts are connected to the molecule in these positions.[53,58,62] On the other hand, for all the combinations of contact positions on the molecule that do not correspond to a single long-bond, destructive quantum interference around the Fermi level is observed (cf. Figure 13a).[53,58,62] As mentioned, the weight of the 1,*m*-diradical structures go down as m increases, and correspondingly one also observes (both theoretically and experimentally) a steady decrease in the electron transmission probability as the spacing between the two contact positions on the molecule becomes bigger. As such, one can conclude empirically that *the weights of the specific diradicaloid structures, i.e., the extent of electronic coupling between the different couples of potential contact sites, gauges the magnitude of the transmission probability around the Fermi level* as well.

As we have argued before, the long-range electronic coupling along the main conjugation path observed for linear polyenes is in sharp contrast to what is observed for the dendralenes. In these compounds, the cross-conjugation structural motifs restrict structures belonging to the $R(1)$ block to within a single butadienic unit and long-range delocalization along the central C−C backbone is essentially negligible/nonexistent in these compounds. As such, the presence of a cross-conjugation feature can be understood to essentially break the "electronic coupling" between adjacent butadienic units abruptly. Accordingly, one observes QI upon connection of the contacts on opposite sides of this structural feature in a molecular conduction experiment (cf. Figure 13a).[53,58,62]

These findings, arising from a pure and unbiased ab initio VB treatment, corroborate further the many rules for the prediction of quantum interference features constructed from tight-binding models which have been proposed over the past few years.[53,57−60,63,64,67]

More generally speaking, our observation that the wave function of polyenes essentially consists only of $R(0)$ and $R(1)$ structures is in full agreement with the "arrow-pushing" mnemonic central to resonance theory in organic chemistry, which has recently also found its way into the realm of molecular electronics.[62] Indeed, curly arrow drawings are a handy tool to decide whether two sites in a conjugated system can be connected through a single long-bond, thus indicating whether or not these sites are electronically coupled (cf. Figure 13b). In this regard, we also want to refer to the recent work by Gerald Knizia and his co-workers (as well as by others[84]) in which the physical roots of curly arrows have been scrutinized and a quantum chemical method has been developed and embedded into TURBOMOLE[85] to probe their paths throughout chemical reactions.[86,87]

Furthermore, our findings enable us to understand the mechanism behind the barrier effect of cross-conjugation features described in a recent study by one of the authors (T.S.) in which the local current through hydrocarbons was examined. Indeed, cross-conjugation features can essentially seal off specific parts of the polyene molecule for delocalization from either of the contact sites by destroying all electronic coupling between sites on opposite side of this feature (Figure 14; it is no longer possible to draw an $R(1)$ structure connecting sites on opposite sides of the feature).[18]

Additionally, our observation, laid out in the second paragraph of this section, that the magnitude of the transmission probability around the Fermi level for a specific configuration of contacts on the molecule appears to be governed by the weight of the corresponding diradical structure in the wave function corroborates in a more quantitative manner *the previously proposed diradical character rule* to estimate the magnitude of

DOI: 10.1021/jacs.9b01420
J. Am. Chem. Soc. 2019, 141, 6030−6047

conductance through molecules under small bias.[88−90] The posited connection between the magnitude of the transmission probability and the weight of the diradical structures also explains the extraordinarily high transmission probabilities calculated for molecular electronic devices in which contacts are connected to exocyclic methylene groups in *p*-QDM:[91,92] two $R(1)$ structures connect these two sites, and their combined weight is higher than that of any other 1,6- or 1,8-connection considered in this study.

5. CONCLUSIONS

In this study, we examined the nature of the electronic structure of some representative cross-conjugated polyenes from a VB perspective. We performed VBSCF calculations on both dendralenes and quinodimethane compounds and found a stark contrast in the delocalization features among them. Dendralenes exhibit impeded delocalization along their C−C backbone; they can essentially be considered as a set of disjointed butadiene units. Quinodimethanes on the other hand exhibit excellent delocalization, even exceeding the extent of delocalization found in linear polyenes. Our subsequent analysis demonstrated that the calculated differences in delocalization can be rationalized based on the relative weights of the specific classes of Rumer structures; only $R(0)$ and $R(1)$ VB structures play a significant role in the wave function, and as such, the number of $R(1)$ structures associated with a specific topology determines the delocalization characteristics of the considered compound. This realization enables us to connect our results to a variety of localization/delocalization-related concepts and rules, central to both organic chemistry and single molecule electronics. Among others, our ab initio VB treatment leads to a lucid rationalization of the apparent relation between cross-conjugated topologies and the occurrence of destructive quantum interference and offers a justification of the recently proposed diradical-character-based rule for the estimation of the magnitude of molecular conductance. More broadly, our results are in full agreement with the often dismissed "arrow-pushing" concept, originating from resonance theory.[93]

■ ASSOCIATED CONTENT

Supporting Information

The Supporting Information is available free of charge on the ACS Publications website at DOI: 10.1021/jacs.9b01420.

Geometries of the linear polyenes, dendralenes, *o*-QDMs, and *p*-QDMs, the appropriate choice of VB orbitals, the generation of Rumer structures for cross-conjugated dendralenes, $\Delta E_{HOMO-LUMO}$ and ΔE_{ST} for the linear and cross-conjugated polyenes, delocalization in the QDM molecules and a comparison of the three families, the VB perturbation energy for calculating the delocalization energy using $R(0)$ as the reference state, comparison of the perturbation energy contributions in the three families, discussion of the conformation of *s-cis* butadiene, VB expansion of the VBSCF(BDO-C) for butadiene, and the Rumer structures in the different blocks (PDF)

■ AUTHOR INFORMATION

Corresponding Authors

*weiwu@xmu.edu.cn
*thijs.stuyver@mail.huji.ac.il
*rh34@cornell.edu
*sason.shaik@gmail.com

ORCID

Wei Wu: 0000-0002-6139-5443
Thijs Stuyver: 0000-0002-8322-0572
Roald Hoffmann: 0000-0001-5369-6046
Yuta Tsuji: 0000-0003-4224-4532
Sason Shaik: 0000-0001-7643-9421

Notes

The authors declare no competing financial interest.

■ ACKNOWLEDGMENTS

T.S. acknowledges the Research Foundation-Flanders (FWO) for a position as postdoctoral research fellow (Grant 1203419N). S.S. is supported by the Israel Science Foundation (Grant ISF 520/18). W.W. is supported by the Natural Science Foundation of China (Grant 21733008). J.G. is thankful for the research fund from Xiamen University (Grant 20720180025). Y.T. thanks Research Institute for Information Technology (Kyushu University) for the computer facilities and financial support from JSPS KAKENHI Grants JP17K14440 and JP18H04488. The paper is dedicated to Klaus Ruedenberg on the occasion of his forthcoming 100th birthday.

■ REFERENCES

(1) Hopf, H., Sherburn, M. S., Eds. *Cross Conjugation: Modern Dendralene, Radialene and Fulvene Chemistry*; John Wiley & Sons: Hoboken, NJ, 2016.

(2) Hosoya, H. Cross-conjugation at the heart of understanding the electronic theory of organic chemistry. *Curr. Org. Chem.* **2015**, *19*, 293−310.

(3) Phelan, N. F.; Orchin, M. Cross conjugation. *J. Chem. Educ.* **1968**, *45*, 633−637.

(4) Limacher, P. A.; Lüthi, H. P. Cross-conjugation. *Wiley Interdisciplinary Reviews: Computational Molecular Science* **2011**, *1*, 477−486.

(5) van Walree, C. A.; Kaats-Richters, V. E. M.; Veen, S. J.; Wieczorek, B.; van der Wiel, J. H.; van der Wiel, B. C. Charge-transfer interactions in 4-donor 4′-acceptor substituted 1,1-diphenylethenes. *Eur. J. Org. Chem.* **2004**, *2004*, 3046−3056.

(6) Tykwinski, R. R.; Schreiber, M.; Carlón, R. P.; Diederich, F.; Gramlich, V. Donor/acceptor-substituted tetraethynylethenes: Systematic assembly of molecules for use as advanced materials. *Helv. Chim. Acta* **1996**, *79* (8), 2249−2281.

(7) Gu, J.; Wu, W.; Danovich, D.; Hoffmann, R.; Tsuji, Y.; Shaik, S. Valence bond theory reveals hidden delocalized diradical character of polyenes. *J. Am. Chem. Soc.* **2017**, *139*, 9302−9316.

(8) Guédon, C. M.; Valkenier, H.; Markussen, T.; Thygesen, K. S.; Hummelen, J. C.; Van Der Molen, S. J. Observation of quantum interference in molecular charge transport. *Nat. Nanotechnol.* **2012**, *7*, 305−309.

(9) Valkenier, H.; Guédon, C. M.; Markussen, T.; Thygesen, K. S.; van der Molen, S. J.; Hummelen, J. C. Cross-conjugation and quantum interference: A general correlation? *Phys. Chem. Chem. Phys.* **2014**, *16*, 653−662.

(10) Solomon, G. C.; Andrews, D. Q.; Goldsmith, R. H.; Hansen, T.; Wasielewski, M. R.; Van Duyne, R. P.; Ratner, M. A. Quantum interference in acyclic systems: Conductance of cross-conjugated molecules. *J. Am. Chem. Soc.* **2008**, *130*, 17301−17308.

(11) Pedersen, K. G.; Borges, A.; Hedegård, P.; Solomon, G. C.; Strange, M. Illusory connection between cross-conjugation and quantum interference. *J. Phys. Chem. C* **2015**, *119*, 26919−26924.

(12) Hopf, H. The dendralenes—a neglected group of highly unsaturated hydrocarbons. *Angew. Chem., Int. Ed. Engl.* **1984**, *23*, 948−960.

(13) Hopf, H. Dendralenes: The breakthrough. *Angew. Chem., Int. Ed.* **2001**, *40*, 705−707.

DOI: 10.1021/jacs.9b01420
J. Am. Chem. Soc. 2019, 141, 6030−6047

(14) Payne, A. D.; Bojase, G.; Paddon-Row, M. N.; Sherburn, M. S. Practical synthesis of the dendralene family reveals alternation in behavior. *Angew. Chem.* **2009**, *121*, 4930−4933.
(15) Hopf, H.; Sherburn, M. S. Dendralenes branch out: Cross-conjugated oligoenes allow the rapid generation of molecular complexity. *Angew. Chem., Int. Ed.* **2012**, *51*, 2298−2338.
(16) Saglam, M. F.; Fallon, T.; Paddon-Row, M. N.; Sherburn, M. S. Discovery and computational rationalization of diminishing alternation in [n] dendralenes. *J. Am. Chem. Soc.* **2016**, *138*, 1022−1032.
(17) Almenningen, A.; Gatial, A.; Grace, D. S. B.; Hopf, H.; Klaeboe, P.; Lehrich, F.; Nielsen, C. J.; Powell, D. L.; Traetteberg, M. The molecular structure of 3-methylene-1, 4-pentadiene studied by gas-phase electron diffraction and by vibrational, NMR and ultraviolet spectroscopy. *Acta Chem. Scand.* **1988**, *42a*, 634−650.
(18) Brain, P. T.; Smart, B. A.; Robertson, H. E.; Davis, M. J.; Rankin, D. W.; Henry, W. J.; Gosney, I. Molecular structure of 3, 4-dimethylenehexa-1, 5-diene ([4] dendralene), C8H10, in the gas phase as determined by electron diffraction and ab initio calculations. *J. Org. Chem.* **1997**, *62*, 2767−2773.
(19) Stuyver, T.; Blotwijk, N.; Fias, S.; Geerlings, P.; De Proft, F. Exploring electrical currents through nanographenes: Visualization and tuning of the through-bond transmission paths. *ChemPhysChem* **2017**, *18*, 3012−3022.
(20) Hajgató, B.; Szieberth, D.; Geerlings, P.; De Proft, F.; Deleuze, M. S. A benchmark theoretical study of the electronic ground state and of the singlet-triplet split of benzene and linear acenes. *J. Chem. Phys.* **2009**, *131*, 224321.
(21) Dias, J. R. Properties and relationships of conjugated polyenes having a reciprocal eigenvalue spectrum−Dendralene and radialene hydrocarbons. *Croat. Chem. Acta* **2004**, *77*, 325−330.
(22) Gholami, M.; Tykwinski, R. R. Oligomeric and polymeric systems with a cross-conjugated π-framework. *Chem. Rev.* **2006**, *106*, 4997−5027.
(23) Gineityte, V. A simple rationale for lowered stabilities of branched and cross-conjugated polyenes. *Monatsh. Chem.* **2016**, *147*, 1303−1313.
(24) Dias, J. R. A quantitative metric for conjugation in polyene hydrocarbons having a single classical structure. *J. Phys. Chem. A* **2014**, *118*, 10822−10836.
(25) Limacher, P. A. Electron delocalization in through and cross conjugated oligomers and its influence on the molecular properties. Ph.D. Dissertation, ETH Zurich, Zurich, Switzerland, 2010.
(26) Kertesz, M.; Choi, C. H.; Yang, S. Conjugated polymers and aromaticity. *Chem. Rev.* **2005**, *105*, 3448−3481.
(27) Payne, A. D.; Willis, A. C.; Sherburn, M. S. Practical synthesis and Diels− Alder chemistry of [4] dendralene. *J. Am. Chem. Soc.* **2005**, *127*, 12188−12189.
(28) Auwers, K. V. I. Ueber Alkylidendihydrobenzolderivate. *Justus Liebigs Ann.* **1907**, *352*, 219−272.
(29) Auwers, K. Zur kenntnis hydroaromatischer verbindungen: über chlorderivatc von hydroaromatischen ketonen und semibenzolen. *Ber. Dtsch. Chem. Ges.* **1911**, *44*, 788−809.
(30) Fielder, S.; Rowan, D. D.; Sherburn, M. S. First synthesis of the dendralene family of fundamental hydrocarbons. *Angew. Chem., Int. Ed.* **2000**, *39*, 4331−4333.
(31) Sherburn, M. S. Preparation and synthetic value of π-bond-rich branched hydrocarbons. *Acc. Chem. Res.* **2015**, *48*, 1961−1970.
(32) West, R. Chemistry of the Oxocarbons. *Isr. J. Chem.* **1980**, *20*, 300−307.
(33) Prinzbach, H. Cyclic cross-conjugated π-systems: α, ω-cycloaddition reactions. *Pure Appl. Chem.* **1971**, *28*, 281−330.
(34) Schweikert, O.; Netscher, T.; Knothe, L.; Prinzbach, H. Cyclisch gekreuzt-konjugierte bindungssysteme, 43.(e)-sesquifulvatrien, synthese—thermolyse. *Chem. Ber.* **1984**, *117*, 2027−2044.
(35) Beck, A.; Knothe, L.; Hunkler, D.; Prinzbach, H. Synthesis and 20π-electrocyclisation of heptahendecafulvadiene-An unusual sequence of pericyclic processes. *Tetrahedron Lett.* **1984**, *25*, 1785−1788.
(36) Iyoda, M.; Otani, H.; Oda, M.; Kai, Y.; Baba, Y.; Kasai, N. Octaphenyl [4] radialene. *J. Am. Chem. Soc.* **1986**, *108*, 5371−5372.
(37) Schiess, P.; Heitzmann, M. Hexakis (methylidene)-cyclohexane ("[6] Radialene"). Chemical and spectral properties. *Helv. Chim. Acta* **1978**, *61*, 844−847.
(38) Iyoda, M.; Kuwatani, Y.; Oda, M. Nickel-catalyzed cyclodimerization of [5] cumulene (hexapentaene). Synthesis of a novel [4] radialene system. *J. Am. Chem. Soc.* **1989**, *111*, 3761−3762.
(39) Mackay, E. G.; Newton, C. G.; Toombs-Ruane, H.; Lindeboom, E. J.; Fallon, T.; Willis, A. C.; Paddon-Row, M. N.; Sherburn, M. S. [5] Radialene. *J. Am. Chem. Soc.* **2015**, *137*, 14653−14659.
(40) Neuenschwander, M. Fulvenes. *Double-Bonded Functional Groups*; Wiley & Sons: Hoboken, NJ, 1989; pp 1131−1268, DOI: 10.1002/9780470772256.ch4.
(41) Brunmark, A.; Cadenas, E. Redox and addition chemistry of quinoid compounds and its biological implications. *Free Radical Biol. Med.* **1989**, *7*, 435−477.
(42) Squadrito, G. L.; Cueto, R.; Dellinger, B.; Pryor, W. A. Quinoid redox cycling as a mechanism for sustained free radical generation by inhaled airborne particulate matter. *Free Radical Biol. Med.* **2001**, *31*, 1132−1138.
(43) Powis, G. Metabolism and reactions of quinoid anticancer agents. *Pharmacol. Ther.* **1987**, *35*, 57−162.
(44) McCoull, K. D.; Rindgen, D.; Blair, I. A.; Penning, T. M. Synthesis and characterization of polycyclic aromatic hydrocarbon o-quinone depurinating N7-guanine adducts. *Chem. Res. Toxicol.* **1999**, *12*, 237−246.
(45) Pathak, T. P.; Sigman, M. S. Applications of ortho-quinone methide intermediates in catalysis and asymmetric synthesis. *J. Org. Chem.* **2011**, *76*, 9210−9215.
(46) Rosenau, B.; Krieger, C.; Staab, H. A. Sterically crowded tetracyano-para-quinodimethanes: synthesis and structure of 2, 3, 5, 6-tetramethyl-7, 7, 8, 8-tetracyano-para-quinodimethane. *Tetrahedron Lett.* **1985**, *26*, 2081−2084.
(47) Belik, P.; Gügel, A.; Spickermann, J.; Müllen, K. Reaction of buckminsterfullerene with ortho-quinodimethane: A new access to stable C60 derivatives. *Angew. Chem., Int. Ed. Engl.* **1993**, *32*, 78−80.
(48) Shimizu, A.; Tobe, Y. Indeno [2, 1-a] fluorene: An air-stable ortho-quinodimethane derivative. *Angew. Chem.* **2011**, *123*, 7038−7042.
(49) Fowler, P. W.; Hansen, P.; Caporossi, G.; Soncini, A. Polyenes with maximum HOMO−LUMO gap. *Chem. Phys. Lett.* **2001**, *342*, 105−112.
(50) Zhao, Y.; Slepkov, A. D.; Akoto, C. O.; McDonald, R.; Hegmann, F. A.; Tykwinski, R. R. Synthesis, structure, and nonlinear optical properties of cross-conjugated perphenylated iso-polydiacetylenes. *Chem. - Eur. J.* **2005**, *11*, 321−329.
(51) Sun, L.; Diaz-Fernandez, Y. A.; Gschneidtner, T. A.; Westerlund, F.; Lara-Avila, S.; Moth-Poulsen, K. Single-molecule electronics: From chemical design to functional devices. *Chem. Soc. Rev.* **2014**, *43*, 7378−7411.
(52) Datta, S. *Electronic Transport in Mesoscopic Systems*; Cambridge University Press: Cambridge, U.K., 1995.
(53) Markussen, T.; Stadler, R.; Thygesen, K. S. The relation between structure and quantum interference in single molecule junctions. *Nano Lett.* **2010**, *10*, 4260−4265.
(54) Solomon, G. C.; Andrews, D. Q.; Hansen, T.; Goldsmith, R. H.; Wasielewski, M. R.; Van Duyne, R. P.; Ratner, M. A. Understanding quantum interference in coherent molecular conduction. *J. Chem. Phys.* **2008**, *129*, 054701.
(55) Arroyo, C. R.; Tarkuc, S.; Frisenda, R.; Seldenthuis, J. S.; Woerde, C. H.; Eelkema, R.; Grozema, F. C.; van der Zant, H. S. Signatures of quantum interference effects on charge transport through a single benzene ring. *Angew. Chem.* **2013**, *125*, 3234−3237.
(56) Fracasso, D.; Valkenier, H.; Hummelen, J. C.; Solomon, G. C.; Chiechi, R. C. Evidence for quantum interference in SAMs of arylethynylene thiolates in tunneling junctions with eutectic Ga−In (EGaIn) top-contacts. *J. Am. Chem. Soc.* **2011**, *133*, 9556−9563.
(57) Tsuji, Y.; Estrada, E.; Movassagh, R.; Hoffmann, R. Quantum interference, graphs, walks and polynomials. *Chem. Rev.* **2018**, *118*, 4887−4911.

DOI: 10.1021/jacs.9b01420
J. Am. Chem. Soc. 2019, 141, 6030−6047

(58) Yoshizawa, K.; Tada, T.; Staykov, A. Orbital views of the electron transport in molecular devices. *J. Am. Chem. Soc.* **2008**, *130*, 9406−9413.
(59) Geng, Y.; Sangtarash, S.; Huang, C.; Sadeghi, H.; Fu, Y.; Hong, W.; Wandlowski, T.; Decurtins, S.; Lambert, C.; Liu, S. X. Magic ratios for connectivity-driven electrical conductance of graphene-like molecules. *J. Am. Chem. Soc.* **2015**, *137*, 4469−4476.
(60) Tsuji, Y.; Hoffmann, R.; Movassagh, R.; Datta, S. Quantum interference in polyenes. *J. Chem. Phys.* **2014**, *141*, 224311.
(61) Tsuji, Y.; Stuyver, T.; Gunasekaran, S.; Venkataraman, L. The influence of linkers on quantum interference: A linker theorem. *J. Phys. Chem. C* **2017**, *121*, 14451−14462.
(62) Stuyver, T.; Fias, S.; De Proft, F.; Geerlings, P. Back of the envelope selection rule for molecular transmission: A curly arrow approach. *J. Phys. Chem. C* **2015**, *119*, 26390−26400.
(63) Tsuji, Y.; Yoshizawa, K. Frontier orbital perspective for quantum Interference in alternant and nonalternant hydrocarbons. *J. Phys. Chem. C* **2017**, *121*, 9621−9626.
(64) Stuyver, T.; Fias, S.; De Proft, F.; Fowler, P. W.; Geerlings, P. (2015). Conduction of molecular electronic devices: Qualitative insights through atom-atom polarizabilities. *J. Chem. Phys.* **2015**, *142*, 094103.
(65) Stuyver, T.; Fias, S.; Geerlings, P.; De Proft, F.; Alonso, M. Qualitative insights into the transport properties of hückel/möbius (anti) aromatic compounds: Application to expanded porphyrins. *J. Phys. Chem. C* **2018**, *122*, 19842−19856.
(66) Su, T. A.; Neupane, M.; Steigerwald, M. L.; Venkataraman, L.; Nuckolls, C. Chemical principles of single-molecule electronics. *Nat. Rev. Mater.* **2016**, *1*, 16002.
(67) Tsuji, Y.; Hoffmann, R.; Strange, M.; Solomon, G. C. Close relation between quantum interference in molecular conductance and diradical existence. *Proc. Natl. Acad. Sci. U. S. A.* **2016**, *113*, E413−E419.
(68) (a) Becke, A. D. Density-functional thermochemistry. III. The role of exact exchange. *J. Chem. Phys.* **1993**, *98*, 5648−5652. (b) Stephens, P. J.; Devlin, F. J.; Chabalowski, C. F.; Frisch, M. J. Ab initio calculation of vibrational absorption and circular dichroism spectra using density functional force fields. *J. Phys. Chem.* **1994**, *98*, 11623−11627. (c) Frish, M. J.; Trucks, G. W.; Schlegel, H. B.; Scuseria, G. E.; Robb, M. A.; Cheeseman, J. R.; Scalmani, G.; Barone, V.; Mennucci, B.; Petersson, G. A.; Nakatsuji, H.; Caricato, M.; Li, X.; Hratchian, H. P.; Izmaylov, A. F.; Bloino, J.; Zheng, G.; Sonnenberg, J. L.; Hada, M.; Ehara, M.; Toyota, K.; Fukuda, R.; Hasegawa, J.; Ishida, M.; Nakajima, T.; Honda, Y.; Kitao, O.; Nakai, H.; Vreven, T.; Montgomery, J. A., Jr.; Peralta, J. E.; Ogliaro, F.; Bearpark, M.; Heyd, J. J.; Brothers, E.; Kudin, K. N.; Staroverov, V. N.; Keith, T.; Kobayashi, R.; Normand, J.; Raghavachari, K.; Rendell, A.; Burant, J. C.; Iyengar, S. S.; Tomasi, J.; Cossi, M.; Rega, N.; Millam, J. M.; Klene, M.; Knox, J. E.; Cross, J. B.; Bakken, V.; Adamo, C.; Jaramillo, J.; Gomperts, R.; Stratmann, R. E.; Yazyev, O.; Austin, A. J.; Cammi, R.; Pomelli, C.; Ochterski, J. W.; Martin, R. L.; Morokuma, K.; Zakrzewski, V. G.; Voth, G. A.; Salvador, P.; Dannenberg, J. J.; Dapprich, S.; Daniels, A. D.; Farkas, O.; Foresman, J. B.; Ortiz, J. V.; Cioslowski, J.; Fox, D. J. *Gaussian 09*, revision D.01; Gaussian, Inc.: Wallingford, CT, 2013.
(69) Dunning, T. H.; Hay, P. J. In *Modern Theoretical Chemistry*; Schaefer, H. F., III, Ed.; Plenum Press: New York, 1977, Vol. 3, pp 1−28.
(70) (a) van Lenthe, J. H.; Balint-Kurti, G. G. The valence-bond scf (VB SCF) method.: Synopsis of theory and test calculation of oh potential energy curve. *Chem. Phys. Lett.* **1980**, *76*, 138−142. (b) van Lenthe, J. H.; Balint-Kurti, G. G. The valence-bond self-consistent field method (VB−SCF): Theory and test calculations. *J. Chem. Phys.* **1983**, *78*, 5699−5713. (c) Verbeek, J.; van Lenthe, J. H. On the evaluation of non-orthogonal matrix elements. *J. Mol. Struct.: THEOCHEM* **1991**, *229*, 115−137.
(71) (a) Song, L.; Chen, Z.; Ying, F.; Song, J.; Chen, X.; Su, P.; Mo, Y.; Zhang, Q.; Wu, W. *XMVB 2.0: An Ab Initio Non-Orthogonal Valence Bond Program*; Xiamen University (Xiamen 361005, China), 2012. (b) Song, L.; Mo, Y.; Zhang, Q.; Wu, W. XMVB: A program for ab initio nonorthogonal valence bond computations. *J. Comput. Chem.* **2005**, *26* (5), 514−521. (c) Chen, Z.; Ying, F.; Chen, X.; Song, J.; Su, P.; Song, L.; Mo, Y.; Zhang, Q.; Wu, W. XMVB 2.0: A new version of Xiamen valence bond program. *Int. J. Quantum Chem.* **2015**, *115*, 731−737.
(72) Hehre, W. J.; Stewart, R. F.; Pople, J. A. self-consistent molecular-orbital methods. i. use of gaussian expansions of Slater-type atomic orbitals. *J. Chem. Phys.* **1969**, *51*, 2657−2664.
(73) Dunning, T. H., Jr Gaussian basis sets for use in correlated molecular calculations. I. The atoms boron through neon and hydrogen. *J. Chem. Phys.* **1989**, *90*, 1007−1023.
(74) Shaik, S.; Hiberty, P. C. *A Chemist's Guide to Valence Bond Theory*; John Wiley & Sons Inc.: New York, 2008; pp 104−109.
(75) Mo, Y.; Lin, Z.; Wu, W.; Zhang, Q. Bond-distorted orbitals and effects of hybridization and resonance on C−C bond lengths. *J. Phys. Chem.* **1996**, *100*, 11569−11572.
(76) The "atomic orbitals" for a particular atom in VBSCF(BDO) are Coulson−Fisher type AOs, which include delocalization tails on the atoms to which the particular atom is bonded. In this manner the ionic structures are embedded into the covalent structures. BOVB, on the other hand, treats the ionic and covalent structures explicitly and allows each structure to adapt its own orbitals within the SCF procedure.
(77) Su, P.; Li, H. Energy decomposition analysis of covalent bonds and intermolecular interactions. *J. Chem. Phys.* **2009**, *131*, 014102.
(78) Su, P.; Jiang, Z.; Chen, Z.; Wu, W. Energy decomposition scheme based on the generalized Kohn−Sham scheme. *J. Phys. Chem. A* **2014**, *118*, 2531−2542.
(79) Baraban, J. H.; Martin-Drumel, M. A.; Changala, P. B.; Eibenberger, S.; Nava, M.; Patterson, D.; Stanton, J. F.; Ellison, G. B.; McCarthy, M. C. The molecular structure of gauche-1, 3-butadiene: experimental establishment of non-planarity. *Angew. Chem., Int. Ed.* **2018**, *57*, 1821−1825.
(80) Trinquier, G.; Malrieu, J. P. Kekulé versus Lewis: When aromaticity prevents electron pairing and imposes polyradical character. *Chem. - Eur. J.* **2015**, *21*, 814−828.
(81) Poidevin, C.; Malrieu, J. P.; Trinquier, G.; Lepetit, C.; Allouti, F.; Alikhani, M. E.; Chauvin, R. Towards magnetic carbo-meric molecular materials. *Chem. - Eur. J.* **2016**, *22*, 5295−5308.
(82) Wu, W.; Danovich, D.; Shurki, A.; Shaik, S. Using Valence bond theory to understand electronic excited states: Application to the hidden excited state (2^1Ag) of $C_{2n}H_{2n+2}$ (n= 2− 14) polyenes. *J. Phys. Chem. A* **2000**, *104*, 8744−8758.
(83) Libit, L.; Hoffmann, R. Detailed orbital theory of substituent effects. Charge transfer, polarization, and the methyl group. *J. Am. Chem. Soc.* **1974**, *96*, 1370−1383.
(84) Liu, Y.; Kilby, P.; Frankcombe, T. J.; Schmidt, T. W. Calculating curly arrows from ab initio wavefunctions. *Nat. Commun.* **2018**, *9*, 1436.
(85) Ahlrichs, R.; Bär, M.; Häser, M.; Horn, H.; Kölmel, C. Electronic structure calculations on workstation computers: The program system turbomole. *Chem. Phys. Lett.* **1989**, *162*, 165−169.
(86) Knizia, G.; Klein, J. E. Electron Flow in reaction mechanisms—revealed from first principles. *Angew. Chem., Int. Ed.* **2015**, *54*, 5518−5522.
(87) Klein, J. E.; Knizia, G. cPCET versus HAT: A Direct theoretical method for distinguishing X−H Bond-activation mechanisms. *Angew. Chem.* **2018**, *130*, 12089−12093.
(88) Stuyver, T.; Fias, S.; De Proft, F.; Geerlings, P.; Tsuji, Y.; Hoffmann, R. Enhancing the conductivity of molecular electronic devices. *J. Chem. Phys.* **2017**, *146*, 092310.
(89) Stuyver, T.; Zeng, T.; Tsuji, Y.; Fias, S.; Geerlings, P.; De Proft, F. Captodative substitution: A strategy for enhancing the conductivity of molecular electronic devices. *J. Phys. Chem. C* **2018**, *122*, 3194−3200.
(90) Stuyver, T.; Zeng, T.; Tsuji, Y.; Geerlings, P.; De Proft, F. Diradical character as a guiding principle for the insightful design of molecular nanowires with an increasing conductance with length. *Nano Lett.* **2018**, *18*, 7298−7304.
(91) Ramos-Berdullas, N.; Mandado, M. Electronic properties of p-xylylene and p-phenylene chains subjected to finite bias voltages: a new highly conducting oligophenyl structure. *Chem. - Eur. J.* **2013**, *19*, 3646−3654.

DOI: 10.1021/jacs.9b01420
J. Am. Chem. Soc. 2019, 141, 6030−6047

(92) Stuyver, T.; Fias, S.; De Proft, F.; Geerlings, P. The relation between delocalization, long bond order structure count and transmission: An application to molecular wires. *Chem. Phys. Lett.* **2015**, *630*, 51−56.
(93) Alvarez, S. A. Chemistry: A panoply of arrows. *Angew. Chem., Int. Ed.* **2012**, *51*, 590−600.

DOI: 10.1021/jacs.9b01420
J. Am. Chem. Soc. 2019, 141, 6030−6047